Quaternary Science Reviews 345 (2024) 109055

Contents lists available at ScienceDirect

Quaternary Science Reviews

journal homepage: www.elsevier.com/locate/quascirev

The role of ocean circulation and regolith removal in triggering the Mid-Pleistocene Transition: Insights from authigenic Nd isotopes

Thomas J. Williams [a,b,c,d,*], Alexander M. Piotrowski [c], Jacob N.W. Howe [c], Claus-Dieter Hillenbrand [d], Claire S. Allen [d], Josephine A. Clegg [c]

[a] Institute for Marine and Antarctic Studies, University of Tasmania, Hobart, TAS, Australia
[b] The Australian Centre for Excellence in Antarctic Science, University of Tasmania, Hobart, TAS, Australia
[c] Department of Earth Sciences, Cambridge University, Cambridge, UK
[d] British Antarctic Survey, Cambridge, UK

ARTICLE INFO

Handling editor: A. Voelker

ABSTRACT

Approximately 1,250,000 to 700,000 years ago, the pacing of glacial-interglacial cycles changed from 41,000 years to ~100,000 years, a shift known as the 'Mid-Pleistocene Transition' (MPT). The cause – or causes – of this shift remain uncertain. However, changes in ocean circulation and removal of northern hemisphere regolith have both been proposed as potential triggers. Here, we present continuous, orbitally resolved reconstructions of deep ocean neodymium isotopes from three locations in the equatorial Atlantic, Indian and southwest Pacific oceans, spanning 1.7 million years from the Holocene to before the MPT, to test these two hypotheses. We find that global seawater neodymium isotope variability over glacial-interglacial cycles is controlled by changes in both neodymium input to the North Atlantic and deep ocean mixing. Using this neodymium isotope data, we show that enhanced northern hemisphere regolith removal began approximately 1.45 million years ago, ~200,000 years prior to the onset of the MPT and ~500,000 years prior to a major expansion in northern hemisphere ice sheets between ~900,000 and 870,000 years ago. This ice sheet expansion was immediately preceded by an interval of reduced mixing of Atlantic-sourced waters into the deep southwest Pacific Ocean. We hypothesize that this circulation reorganization reflected increased stratification of the deep Southern Ocean interior, possibly in response to cooling and Antarctic sea ice expansion at this time. Taken together, these data suggest an expansion and/or thickening of northern hemisphere ice sheets during the MPT was facilitated by a combination of reduced northern hemisphere regolith cover alongside Southern Ocean circulation changes. Together, these shifts allowed the build up of larger northern hemisphere ice sheets that were more resistant to deglaciation, facilitating the longer glacial cycles of the post-MPT world.

1. Introduction

1.1. The mid pleistocene transition

The Quaternary period (0–2.58 million years ago [Ma]) is characterized by a series of around 50 glacial periods, alternating with warmer interglacial periods. The rhythm of these glacial-interglacial cycles is ultimately paced by insolation changes, caused by cyclical variations in the Earth's orbit. The Mid-Pleistocene Transition (MPT) marks a shift from obliquity-paced 41 thousand year (kyr) glacial-interglacial cycles to longer cycles averaging ~100 kyr. This transition occurred sometime between 1250–700 thousand years ago (ka) and does not correspond to changes in external insolation forcing, rather the response of the climate system to this forcing (e.g. Barker et al., 2022). Following the MPT, glaciations became more intense, with cooler temperatures (Clark et al., 2024) and the build-up of larger ice sheets (Elderfield et al., 2012; Rohling et al., 2014; Ford and Raymo, 2019; Köhler and van de Wal, 2020; Miller et al., 2020; An et al., 2024). Despite decades of research, the cause – or causes – of the MPT remain an enduring mystery of Quaternary climatology (Berends et al., 2021).

Theories seeking to explain the cause(s) of the MPT include two main groups of hypotheses. The first group invokes a step change in the build-up of northern hemisphere ice sheets, which became larger and/or more resistant to deglaciation, allowing for longer and more severe glaciations

* Corresponding author. Institute for Marine and Antarctic Studies, University of Tasmania, Hobart, TAS, Australia.
E-mail address: tom.williams@utas.edu.au (T.J. Williams).

https://doi.org/10.1016/j.quascirev.2024.109055
Received 25 February 2024; Received in revised form 27 October 2024; Accepted 27 October 2024
Available online 6 November 2024

lasting up to ~60 kyr (Clark and Pollard, 1998; Ganopolski and Calov, 2011; Willeit et al., 2019; Yehudai et al., 2021). The 'regolith hypothesis' (Clark and Pollard, 1998) falls into this category and proposes a transition in the substrate upon which these ice sheets grew, from low-friction regolith to high-friction crystalline bedrock, allowing for the build-up of thicker, more resilient ice sheets. A second group implies changes in ocean circulation and/or ocean biogeochemical cycling, which ultimately resulted in the sequestration of greater quantities of carbon within the glacial ocean interior, lowering atmospheric CO_2 and thus allowing for longer, more severe glaciations (Chalk et al., 2017; Kim et al., 2021; Lear et al., 2016; Pena and Goldstein, 2014; Yehudai et al., 2021; Clark et al., 2024). In particular, a change in reconstructed seawater neodymium isotope ratios within the southern Atlantic is attributed to a collapse in the production of North Atlantic sourced waters (NSW) and an expansion of Southern Ocean sourced waters during Marine Isotope Stages (MIS) 23–22 (917–866 ka) (Kim et al., 2021; Pena and Goldstein, 2014), a key interval of northern hemisphere ice sheet expansion.

A number of other, often interrelated, hypotheses explaining the MPT exists, including: an expansion of Antarctic ice sheets, with the large East Antarctic Ice Sheet becoming marine-terminating (Raymo et al., 2006; Elderfield et al., 2012; Ford and Raymo, 2019; An et al., 2024), resulting in increased sensitivity in northern hemisphere-driven sea level variability (Raymo et al., 2006) and/or greater glacial-interglacial variability in Southern Ocean sea ice extent (Clark et al., 2024) and increased moisture transfer to the high latitude northern hemisphere (An et al., 2024); a strengthening of the Southern Ocean halocline, leading to a reduced potential for CO_2 outgassing from upwelled circumpolar waters (Rodriguez-Sanz et al., 2012; Hasenfratz et al., 2019); changing Artic sea ice growth patterns, resulting in reduced moisture transport to northern hemisphere ice sheets and increased ocean albedo during key periods of ice sheet growth and retreat (Gildor and Tziperman, 2001); and a strengthening of the North Atlantic Current, modulating moisture supply to northern hemisphere ice sheets (Barker et al., 2021). These hypotheses share many characteristics, and none are mutually exclusive (Chalk et al., 2017; Willeit et al., 2019; Berends et al., 2021), often invoking a non-linear response to the long-term, CO_2-driven cooling observed throughout the late Cenozoic (Clark et al., 2024). A recurring theme in many hypotheses is a sharp increase in northern hemisphere ice volume across the MPT. However, debate remains around whether northern hemisphere ice sheet expansion was a direct trigger of the MPT, or occurred in response to other climate drivers (An et al., 2024). In this study, we address this debate using three new globally distributed reconstructions of deep ocean neodymium isotopes spanning up to the last 1.7 million years.

1.2. Global seawater ε_{Nd} variability

Neodymium isotopes are typically expressed as $\varepsilon_{Nd} = [(^{143}Nd/^{144}Nd)_{sample}/(^{143}Nd/^{144}Nd)_{CHUR} - 1] \times 10{,}000$, whereby CHUR (Chondritic Uniform Reservoir) is 0.512638 (Jacobsen and Wasserburg, 1980). Within the modern oceans, ε_{Nd} of seawater can be used to trace the flow of different water masses over large distances (e.g. Wu et al., 2022), with ε_{Nd} variability primarily driven by mixing between different water masses (Tachikawa et al., 2017; van de Flierdt et al., 2016; Pöppelmeier et al., 2022; Rahlf et al., 2020; Griffithis et al., 2024; Robinson et al., 2023; Wang et al., 2021; Yehudai et al., 2023; Pasquier et al., 2022). Addition, removal and internal cycling of Nd can also cause changes in seawater ε_{Nd} at some locations, particularly along ocean margins, and these changes can subsequently be traced downstream (Lacan and Jeandel, 2005; Blaser et al., 2020; Filippova et al., 2017; Pöppelmeier et al., 2020a). Processes modulating seawater ε_{Nd} include release of sedimentary Nd into pore waters, and subsequently into bottom waters, during early diagenesis (Abbott et al., 2015a; Du et al., 2020, 2022; Blaser et al., 2020), as well as reversable scavenging of Nd onto sinking particles (Robinson et al., 2023). The former process – termed 'benthic flux' – can alter bottom water ε_{Nd}, while the latter can cause downward migration of Nd isotope signatures, causing a vertical displacement or 'blurring' of water mass boundaries (Pöppelmeier et al., 2022; Wang et al., 2021). These processes are discussed in more detail in Subsection 3.1 below. Because of this, authigenic ε_{Nd} is often described as a 'quasi-conservative' tracer of ocean circulation, sensitive to changes in both ocean circulation and processes impacting seawater ε_{Nd}. Reconstructions of seawater ε_{Nd} can therefore inform us on past changes in both ocean circulation and inputs of Nd (Pöppelmeier et al., 2020b).

The ε_{Nd} signature of present-day North Atlantic Deep Water (NADW, referred to as Northern Sourced Water [NSW] during the past) is characterized by very negative values of ~ -13.2 (Lambelet et al., 2016). The ε_{Nd} signature of NADW largely reflects mixing of Labrador Sea Water, which is characterized by very low ε_{Nd} values (−14.3 to −14.2) (Filippova et al., 2017; Lambelet et al., 2016), with waters sourced within the Nordic Seas that have more positive ε_{Nd} values (~-8.3) (Lambelet et al., 2016; van de Flierdt et al., 2016). The ε_{Nd} signatures of these waters result from the variable continental geology surrounding their areas of formation (Fig. 1). The surrounding geology controls the ε_{Nd} of both dissolved and detrital inputs to the ocean, which in turn impacts ε_{Nd} of seawater in regions of deep water formation (e.g. within the Nordic Seas and Labrador Sea, see Fig. 1 inset) (Blaser et al., 2020). Dissolved riverine Nd inputs (Goldstein and Jacobs, 1987), release of Nd from detrital particles within the water column, reversable scavenging (Wang et al., 2021; Robinson et al., 2023), boundary exchange (Lacan and Jeandel, 2005), and benthic fluxes (Abbott et al., 2015b; Blaser et al., 2020) of Nd between sediments, porewaters and seawater may all play a role in determining the final ε_{Nd} of North Atlantic seawater before it flows south as NADW. Once flowing southward, ε_{Nd} of NADW largely behaves conservatively; that is to say, changes in ε_{Nd} are dominated by mixing between water masses, rather than Nd addition or internal cycling within the water column (Tachikawa et al., 2017; van de Flierdt et al., 2016; Wu et al., 2022). The very negative ε_{Nd} of NADW contrasts with the more positive ε_{Nd} values of Pacific-sourced waters, with ε_{Nd} of Pacific Deep Water (PDW) ranging from ~-4 to −2 (Behrens et al., 2018) (Fig. 1). This pattern of global seawater ε_{Nd} leads to a roughly binary mixing curve within the global ocean, from ε_{Nd} values of ~ -13.2 in the North Atlantic to approximately −4 to −2 within the deep Pacific, with Southern Ocean Circumpolar Deep Water (CDW, ε_{Nd} ~ -8) largely reflecting a mixture of these two sources, with a major contribution from NADW (van de Flierdt et al., 2016; Pasquier et al., 2022) (Fig. 1). Mixing with Antarctic Bottom Water (AABW) also modifies the ε_{Nd} signature of NADW and CDW within the South Atlantic and Southern Ocean (van de Flierdt et al., 2016).

1.3. Study site selection

To capture past changes in global seawater neodymium isotope ratios, we reconstructed paleo-seawater ε_{Nd} using three deep-sea sediment cores retrieved from the equatorial Atlantic (Ocean Drilling Program [ODP] Site 929, 4368 m water depth), equatorial Indian (ODP Site 758, 2935 m water depth) and SW Pacific (ODP Site 1123, 3290 m water depth) oceans (see Subsection 2.1 and Fig. 1). This work extends the previously published ε_{Nd} record of Atlantic ODP Site 929, which spans the last 800 kyr (Howe and Piotrowski, 2017), back to 2.1 Ma (Fig. 2 and S1). We also incorporate previously published low resolution ε_{Nd} data from Indian ODP Site 758 (Burton and Vance, 2000; Gourlan et al., 2010) with our new data from the same core site (Fig. 2 and S1).

The Atlantic site (ODP 929) is today located close to the boundary between NADW and AABW, and is thus sensitive to past changes in Atlantic Meridional Overturning Circulation (AMOC). The Indian Ocean site (ODP 758) is bathed in modified CDW with a relatively high proportion of Atlantic-sourced waters, while the SW Pacific site (ODP 1123) is bathed in Lower CDW, today defined by a salinity maximum attributed to admixture of Atlantic-sourced waters into the deep Southern Ocean. We combine these records with previously published seawater

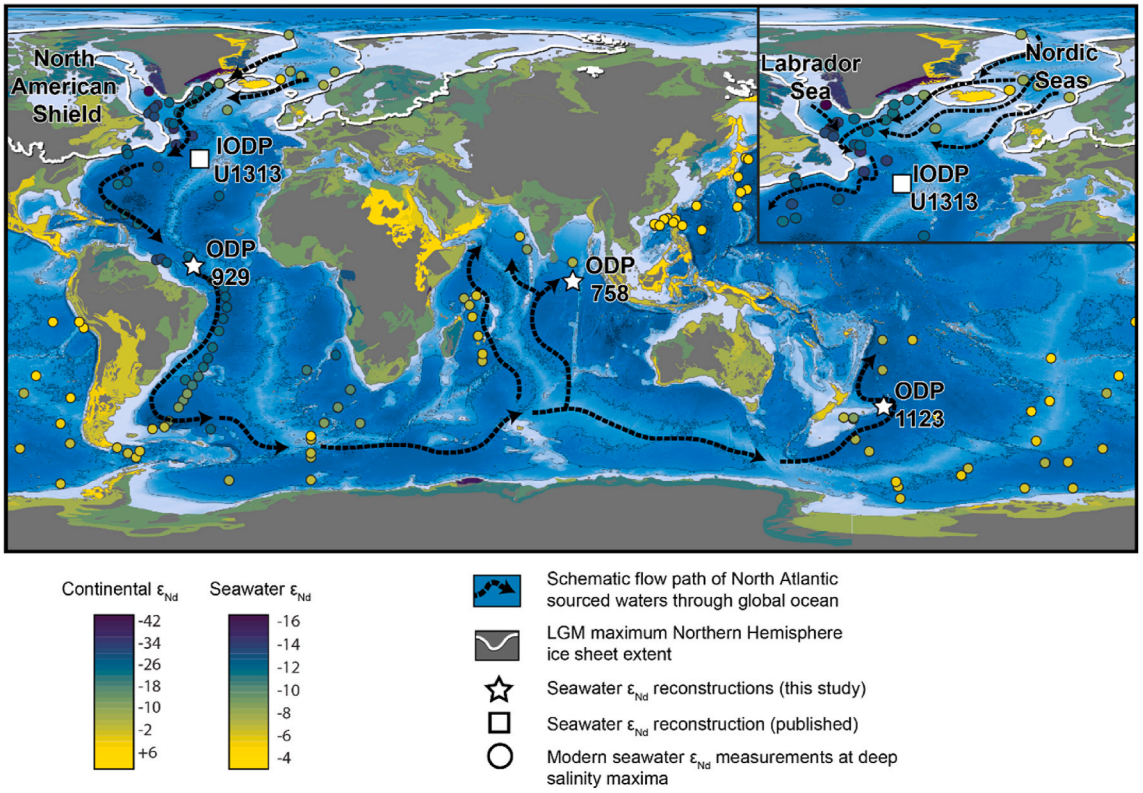

Fig. 1. Global terrestrial and marine ε_{Nd}. Location of core sites presented in this study (white stars) alongside ε_{Nd} of continental margin rocks (Robinson et al., 2021) and deep (>1600 m) seawater stations. Black arrows show schematically the flow path of North Atlantic-sourced waters as they mix through the global ocean, and white line corresponds to northern hemisphere ice-sheet limits at the Last Glacial Maximum (LGM) (Batchelor et al., 2019). Seawater ε_{Nd} data shown are picked from deep salinity maxima, as this can be used to trace North Atlantic Deep Water (NADW) flow. Seawater ε_{Nd} data and references provided in Table S1.

ε_{Nd} reconstructions from the North Atlantic record of Integrated Ocean Drilling Program (IODP) Site U1313 (actually a composite of data from Deep-Sea Drilling Project [DSDP] Site 607 (Kim et al., 2021), core V30-97 (Kim et al., 2021) and IODP Site U1313 (Lang et al., 2016; Lippold et al., 2016; Pöppelmeier et al., 2018, 2021)), which is bathed in newly formed NADW. Together, the ε_{Nd} records from these four locations are well placed to monitor changes in both the ε_{Nd} composition of NSW and its advection through the world ocean via the global thermohaline circulation (Fig. 1).

2. Material and methods

2.1. Marine sediment core locations and chronologies

ODP Site 929 (6.0°N, 43.7°W, water depth: 4368 m) was drilled as part of ODP Leg 154 on the Ceara Rise in the western equatorial Atlantic Ocean (Fig. 1) (Curry et al., 1995). The site lies in the mixing zone between modern NADW and AABW (see Fig. S2). The age model of ODP Site 929 used here is a modification of that published as part of the LR04 'stack' of global benthic foraminifera $\delta^{18}O$ measurements (Lisiecki and Raymo, 2005). We use the updated chronology of Howe and Piotrowski (2017) for the period from 800–0 ka, which was constructed utilizing an additional 37 benthic foraminifera (*Cibicides wuellerstorfi* and *C.* spp.) $\delta^{18}O$ measurements alongside 8 radiocarbon dates measured on planktic foraminifera (*Globigerinoides sacculifer* and *G. ruber*), which we re-calibrated using the Marine20 calibration curve (Heaton et al., 2020). The age model between 2133–800 ka was modified by re-tuning the benthic $\delta^{18}O$ measurements published in deMenocal et al. (1997) and Bickert et al. (1997) to the LR04 stack. The age model deviates from that published in the LR04 stack in two regards: Firstly, between 2070–1952 ka the LR04 age model combined the $\delta^{18}O$ minima of interglacial Marine Isotope Stages (MIS) 75 and 77 into one minimum, centered on glacial MIS 76, which should be present as a $\delta^{18}O$ maximum. We have now separated these $\delta^{18}O$ minima into two interglacial periods, MIS 75 and 77. Secondly, incorporating the age model of Howe and Piotrowski (2017) allowed for a better correlation between the $\delta^{18}O$ record from Site 929 and the LR04 stack for the time interval spanning 381–279 ka (Fig. S1). An updated age model for previously published benthic foraminifera $\delta^{18}O$ data is provided in Table S3.

ODP Site 758 (5.4°N, 90.4°E, water depth: 2935 m) was drilled as part of ODP Leg 121 on the Ninetyeast Ridge in the equatorial Indian Ocean (Fig. 1). Today the core site is bathed in modified CDW sourced from the Southern Ocean. The age model of ODP Site 758 was constructed by tuning the benthic foraminifera (*C. wuellerstorfi*) $\delta^{18}O$ record of Chen et al. (1995) to the LR04 stack. The resulting age model is almost identical to that constructed by Lisiecki and Raymo (2005) for use in the LR04 stack, except for a shift of the $\delta^{18}O$ minimum in MIS 13 to 488 ka (LR04 age model: 491 ka), which brings the $\delta^{18}O$ data into better agreement with the LR04 stack (Fig. S1; updated age model provided in Table S3).

ODP Site 1123 (41.8°S, 171.5°W, water depth: 3290 m) was drilled as part of ODP Leg 181 on Chatham Rise to the east of New Zealand. The site is today bathed in Lower CDW as it flows along a deep western boundary current into the SW Pacific. The age model of ODP Site 1123 was previously published by Elderfield et al. (2012), and was constructed by tuning benthic foraminifera $\delta^{18}O$ measurements (*Uvigerina* spp., corroborated by measurements on *C. wuellerstorfi*) to the LR04 stack (Fig. S1).

The composite of previously published North Atlantic ε_{Nd} records presented in Fig. 2 retains the age models published in their respective studies. For IODP Exp. 306 Site U1313 (41°N, 32.96°W, water depth: 3414 m) the age model is as published in Lang et al. (2016), Lippold et al. (2016) and Pöppelmeier et al. (2021, 2018), using the original age model of Naafs et al. (2013) and Smith et al. (2013). For DSDP Leg 94

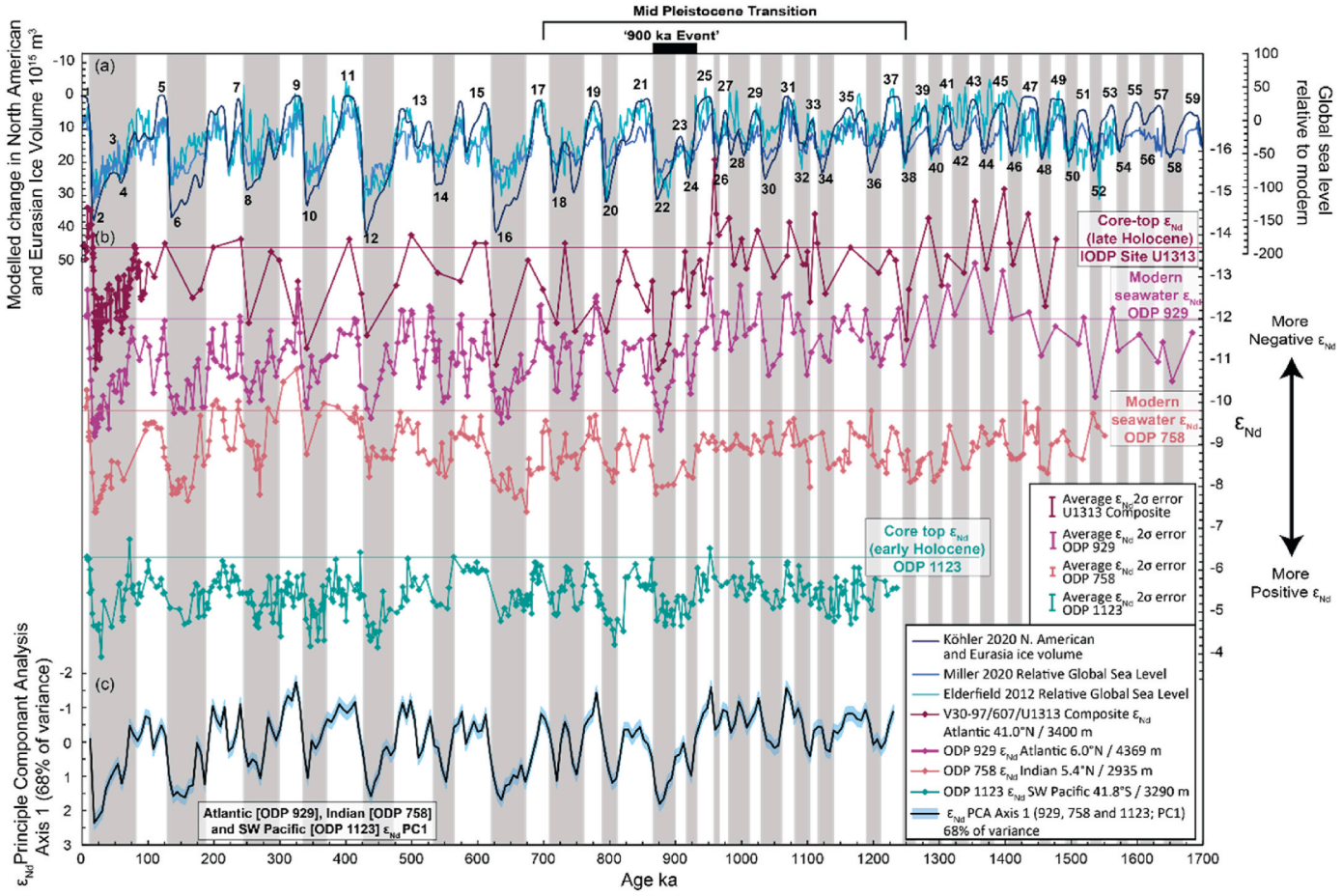

Fig. 2. Global seawater ε_{Nd} since 1.7 Ma. **(a):** Estimates of relative northern hemisphere ice volume and global sea level change (Elderfield et al., 2012; Köhler and van de Wal, 2020; Miller et al., 2020). **(b):** Seawater ε_{Nd} records reconstructed from authigenic fractions of marine sediments from the deep North Atlantic IODP Site U1313 (= composite record comprising DSDP Site 607 (Kim et al., 2021)/core V30-97 (Kim et al., 2021)/IODP Site U1313 (Lang et al., 2016; Lippold et al., 2016; Pöppelmeier et al., 2018, 2021)), equatorial Atlantic ODP Site 929 (Howe and Piotrowski, 2017; this study), equatorial Indian ODP Site 758 (Burton and Vance, 2000; this study) and SW Pacific ODP Site 1123 (Elderfield et al., 2012; this study). **(c):** Axis 1 of Principle Component Analysis (PCA) performed on ODP Site 929, ODP Site 758 and ODP Site 1123, demonstrating shared variance of global seawater ε_{Nd} since ~1.2 Ma. Estimated PC1 uncertainty associated with analytical error shown by blue shading. Marine Isotope Stages (MIS) numbered following Lisiecki and Raymo (2005), with glacial periods shaded in grey.

Site 607 (41°N, 32.95°W, water depth: 3426 m), the age model is as presented in Kim et al. (2021), based on tying of benthic foraminifera $\delta^{18}O$ data to the LR04 stack. For core V30-97 (41°N, 32.93°W, water depth: 3371 m), the age model is as published in Kim et al. (2021), also based on tying of benthic foraminifera $\delta^{18}O$ data to the LR04 stack.

2.2. Reconstructed seawater neodymium isotope ratios (ε_{Nd})

Ancient seawater ε_{Nd} values were extracted from the authigenic Fe-Mn (oxy)hydroxide coatings of bulk sediments from core ODP 758, and the tests of planktic foraminifera from cores ODP 929 and ODP 1123, with additional measurements on fish debris from ODP 929.

The extraction of Fe-Mn (oxy)hydroxide coatings of foraminifera from cores ODP 929 and ODP 1123 was performed following the method of Roberts et al. (2010), using approximately 80 mg of mixed planktic foraminifera. Foraminifera tests were crushed and clays removed via repeated rinsing with milliQ water. Tests were then dissolved in acetic acid. For the extraction of Fe-Mn (oxy)hydroxide coatings from sediments of core ODP 758, a reductive leaching method was employed (Blaser et al., 2016). Approximately 3 g of bulk sediment was leached for 30 min in a 30 mL solution of 0.005 mol/L hydroxylamine hydrochloride and 0.26 mol/L acetic acid. Where insufficient planktic foraminifera were available from ODP 929 sediments, Nd was extracted from fish debris following the methods of Howe and Piotrowski (2017). 15 samples from ODP 929 were selected for paired foraminifera and fish debris ε_{Nd} analyses, of which 12 are within error of one another (Fig. S3). Where duplicate measurements are present, an average ε_{Nd} value and error is used for inclusion in figures and analyses.

Rare earth elements were separated from leachates, dissolved foraminifera and dissolved fish debris using Eichrom TRU spec resin (100–150 μm mesh), and Nd then isolated using Eichrom Ln spec resin (50–100 μm mesh) utilizing volumetrically calibrated columns. Nd isotopes were measured on either a Nu Plasma Inductively Coupled Plasma Mass Spectrometer (ICP-MS) or a Neptune Plus ICP-MS at the Department of Earth Sciences, University of Cambridge (UK). Isotope ratios were corrected for mass dependant fractionation by normalising to $^{146}Nd/^{144}Nd$ of 0.7219 and applying an exponential correction. All samples were bracketed by a concentration matched solution of the reference standard JNdi-1, corrected to $^{143}Nd/^{144}Nd = 0.512115$ (Tanaka et al., 2000). A comparison of paired planktic ε_{Nd} measurements made on both the Nu Plasma ICP-MS and Neptune Plus ICP-MS showed that 56 of 58 samples measured (ε_{Nd} ranged from −13 to −7) agreed within error. 2σ external reproducibility of JNdi-1 standards was between 0.08 and 0.43 epsilon units (n = 203), averaging 0.24 across all runs, while 2σ internal error was between 0.03 and 0.20, averaging 0.08. Errors quoted here are the 2σ reproducibility of the bracketing standard, i.e. external error, except when internal errors were largest. In that case, errors quoted are the combined internal and external errors summed in

quadrate.

2.3. Principal Component Analysis (PCA) of ε_{Nd} data

To determine shared variability – and diagnose potential drivers of this variability – in the ε_{Nd} data presented in this study, PCA was performed on the Nd records of ODP 929, ODP 758 and ODP 1123. ε_{Nd} data were first linearly interpolated at 6 kyr intervals between 1230 ka and 12 ka. ε_{Nd} data were standardized, and PCA performed on the covariance matrix. To test for meaningful correlations, PCA was also performed on randomised ε_{Nd} data from each record, and ranked eigenvalues compared to PCA performed on the real ε_{Nd} data. Ranked eigenvalue 1 of the real ε_{Nd} data was significantly different from the randomised control, however ranked eigenvalues 2 and 3 showed no significant difference. This test demonstrates that only PC1 is significantly different from a randomised time series, and as such PC2 and PC3 are not interpreted here.

To estimate PCA uncertainty associated with ε_{Nd} analytical error, a random error was added or subtracted to each ε_{Nd} measurement, and the PCA performed again, to create synthetic 'error added' principal components. For this, we randomly sampled the average 2σ analytical error from each record, assuming a normal error distribution. PC1 error is then defined as the standard deviation of residuals between the real PC1 scores and 'error added' PC1 score. Error is shown as blue shading in Fig. 2.

2.4. ε_{Nd} binary mixing model

Binary mixing models utilizing geochemical data such as ε_{Nd} are useful in providing an approximation of real-world ocean circulation, with which to test hypotheses for past circulation changes. In particular, they are a useful means to identify large changes in water mass proportions at the global scale (Pöppelmeier et al., 2021, 2023; Yehudai et al., 2023). We therefore applied a binary mixing model utilizing the global ε_{Nd} datasets presented here, to identify changes in global ocean circulation prior to, during and after the MPT.

The largest assumptions in a mixing model concerns the choice of end member ε_{Nd} and water mass Nd concentrations [Nd]. There is currently no proxy for past changes in [Nd], which is almost certain to have changed considerably within the North Atlantic region, due to differential glacial vs. interglacial weathering regimes. However, a recent study tested the impact of variable end member [Nd] on binary mixing calculations and demonstrated that a major impact on results is unlikely (Yehudai et al., 2023). To limit the impact of uncertain end-members, we perform a mixing calculation between NSW and PDW, which captures the global mixing array of ε_{Nd} between highly negative Atlantic waters and more positive Pacific waters. We utilize the composite ε_{Nd} record of IODP Site U1313 (made up of data from core V30-97, DSDP Site 607 and IODP Site U1313) as an approximation of NSW ε_{Nd} in the past. We keep PDW ε_{Nd} fixed at −3.5, as it is thought to have remained largely unchanged at a value of −3 to −4 throughout glacial-interglacial cycles of the Pleistocene (Hu et al., 2016), and potentially for 10s of millions of years (Ling et al., 1997; McKinley et al., 2019). To restrict the potential for missing important features due to interpolating between different time series, we limit the mixing analysis to the MPT (1127–795 ka) and "last glacial cycle" (here defined as 116–6 ka), when the ε_{Nd} record of U1313 has a relatively high temporal resolution.

We interpolate the U1313 ε_{Nd} record to the time steps of the ODP 929, ODP 758 and ODP 1123 records throughout the last glacial cycle, as U1313 is the highest resolution record at that time. We first remove ε_{Nd} data from Heinrich Stadials, as detrital carbonates released by icebergs during Heinrich Events have been shown to alter ε_{Nd} at Site U1313 independent of changes in seawater ε_{Nd} (Blaser et al., 2019; Pöppelmeier et al., 2021). For the MPT, we interpolate the records of ODP 929, ODP 758 and ODP 1123 to the time steps of U1313, as U1313 is the lowest resolution record at that time.

To quantify variability in NSW vs PDW, we utilize equation (1) below:

$$\%NSW = \frac{\varepsilon_{Nd}^{NSW} \bullet [Nd]^{PDW} - \varepsilon_{Nd}^{PDW} \bullet Nd^{PDW}}{\varepsilon_{Nd}^{NSW} \bullet [Nd]^{PDW} - \varepsilon_{Nd}^{PDW} \bullet [Nd]^{PDW} - \varepsilon_{Nd}^{NSW} \bullet [Nd]^{NSW} + \varepsilon_{Nd}^{NSW} \bullet [Nd]^{PDW}} \quad (1)$$

We use modern North Atlantic and Pacific seawater [Nd] values of 18 ppm (Lambelet et al., 2016) and 39 ppm (Amakawa et al., 2009) for [Nd] of NSW and PDW, respectively. Uncertainty is estimated by changing the concentration of NSW by ± 50%.

3. Results and discussion

3.1. Authigenic ε_{Nd} as a tracer of past ocean circulation

In some locations, authigenic ε_{Nd} can be offset from bottom water ε_{Nd} due to release of Nd from detrital phases into sedimentary pore waters, and subsequent incorporation into authigenic phases (e.g. Blaser et al., 2020; Abbott et al., 2022). This pore-water effect may lead to authigenic ε_{Nd} values intermediate between seawater and labile detrital values. This has been documented within seabed surface sediments of the modern Labrador Sea, and may have been more intensive during intervals when large amounts of physically weathered sediment were delivered to this region, e.g. during the early Holocene, when retreating ice caused a large supply of glacially-eroded detritus into the Northwest Atlantic and Labrador Sea (Howe et al., 2016; Blaser et al., 2020). A lack of chemical weathering prior to transport and deposition of glacially eroded and transported sediments may make them more prone to alteration and release of Nd within pore waters. The authigenic fraction of the sediment cores analyzed in this work is not anticipated to be prone to the same contamination by detrital Nd release because the sediments consist mainly of calcareous foraminifera, and therefore the authigenic ε_{Nd} data are interpreted to reflect bottom water ε_{Nd}. This is supported by the lack of offset between core top authigenic and bottom water ε_{Nd} data at sites ODP 929 and ODP 758 (Fig. 2). At Site ODP 1123, an offset between near core-top (30 cm core depth) authigenic ε_{Nd} and SW Pacific bottom water ε_{Nd} data (−6.3 and −8.6, respectively) may reflect the early Holocene (7 ka) – rather than modern – age of these sediments.

Input of detrital Nd into sedimentary pore waters can also lead to changes in overlying bottom waters, in regions where a high elemental flux exists between pore waters and overlying seawater – a so-called benthic flux (Abbott et al., 2015a,b). This can lead to shifts in seawater ε_{Nd} as bottom waters flow across the seafloor (Du et al., 2020, 2022), and may play an important role in setting the final composition of Labrador Sea Water, and subsequently NADW (Blaser et al., 2020; Pöppelmeier et al., 2020a). This non-conservative behavior again appears to mostly occur in regions where predominantly physically weathered sediments and/or particularly reactive sedimentary phases are supplied to the seafloor (Blaser et al., 2020; Pöppelmeier et al., 2020b; Robinson et al., 2023). This is corroborated by the dominance of conservative mixing in seawater ε_{Nd} measurements within the Atlantic Ocean outside the polar regions, i.e., close to sources of mainly chemically weathered sedimentary material (Tachikawa et al., 2017; Du et al., 2020; Wu et al., 2022; Pöppelmeier et al., 2020a; Pöppelmeier et al., 2022; Pasquier et al., 2022).

The absorption and desorption of Nd onto sinking particles within the water column can shift seawater ε_{Nd} values towards that of overlying water masses (Robinson et al., 2023). Known as "reversable scavenging", this process has the potential to offset seawater ε_{Nd} values from those expected during conservative mixing, toward the composition of overlying waters. Recent modelling, utilizing the Nd-enabled Bern3D model, showed that a combination of reversible scavenging and benthic fluxes can lead to an over-estimation of water mass fractions by up to 20% within the Atlantic (Pöppelmeier et al., 2023). Despite these

potential pitfalls, modern seawater ε_{Nd} measurements largely track conservative mixing of water masses along the flow path of the global thermohaline circulation (e.g. Wu et al., 2022, Tachikawa et al., 2017; van de Flierdt et al., 2016), with the largest impact of non-conservative processes observed in specific regions, for example the Labrador Sea (Blaser et al., 2020). Because of this, we expect changes in ε_{Nd} between the core sites studied here to reflect primarily changes in ocean circulation, with non-conservative processes playing a secondary role.

3.2. Glacial-interglacial variability in global seawater ε_{Nd} driven by northern hemisphere climate

Seawater ε_{Nd} reconstructions within the Atlantic, Indian and SW Pacific oceans all show a similar glacial-interglacial cyclicity throughout the last 1700 kyr, with shifts towards more positive ε_{Nd} in each ocean basin during glacials (Fig. 2). The amplitude of these glacial-interglacial shifts was greatest within the Atlantic and Indian oceans, which are located directly 'downstream' of NSW sources. Changes were more muted in the SW Pacific, probably due to mixing with the large volume of PDW. Authigenic ε_{Nd} records form each basin were offset from one another at all times, becoming more positive from the Atlantic towards the SW Pacific, as it is the case for modern seawater ε_{Nd}. Together, these observations suggest that global seawater ε_{Nd} changes likely shared a common driver, while the offset between different ocean basins also suggests continued modulation of seawater ε_{Nd} via mixing between different water masses, as in the modern ocean.

The pacing of glacial-interglacial ε_{Nd} variability largely corresponds to Earth's orbital cycles (Figs. 3 and 4). Prior to approximately 1000 ka, a clear 41 kyr (obliquity) cyclicity existed in the Atlantic and Indian oceans (Fig. 3b). From approximately 1300 ka onwards, an intermittent ~100 kyr (possibly eccentricity) cyclicity emerged in all three ocean basins, which from 750 ka onwards became the dominant cyclicity of global ε_{Nd} changes (Fig. 3a). After 750 ka, the 41 kyr cyclicity can still be observed within the Atlantic and – at times – the Indian and SW Pacific basins. A weak but statistically significant 18–23 kyr (precession) cyclicity was also present within the Atlantic basin at various points throughout the 1700 ka record, becoming more pronounced after ~350 ka (Fig. 3c). The orbital-scale ε_{Nd} cyclicity within each ocean basin was

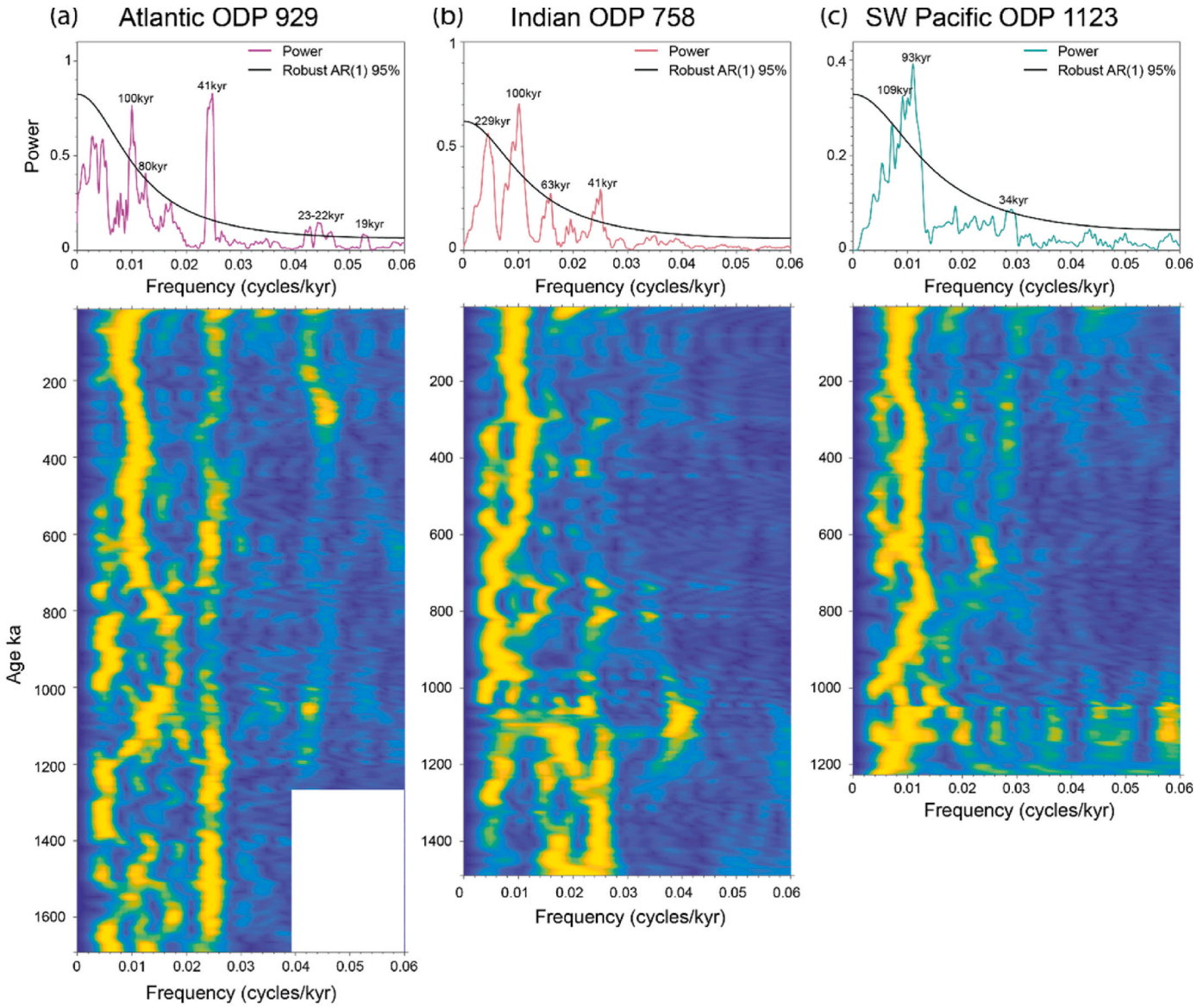

Fig. 3. Seawater ε_{Nd} cyclicities since 1.7 Ma. Spectral power plots (upper) and Fast Fourier Transform analyses (lower) of ε_{Nd} from the deep equatorial Atlantic (**a:** ODP Site 929), Indian (**b:** ODP Site 758) and SW Pacific oceans (**c:** ODP Site 1123). Spectral power peaks above the 95% confidence interval are labelled with corresponding cyclicities. Plotted using Acycle v 2.4.1 (Li et al., 2019).

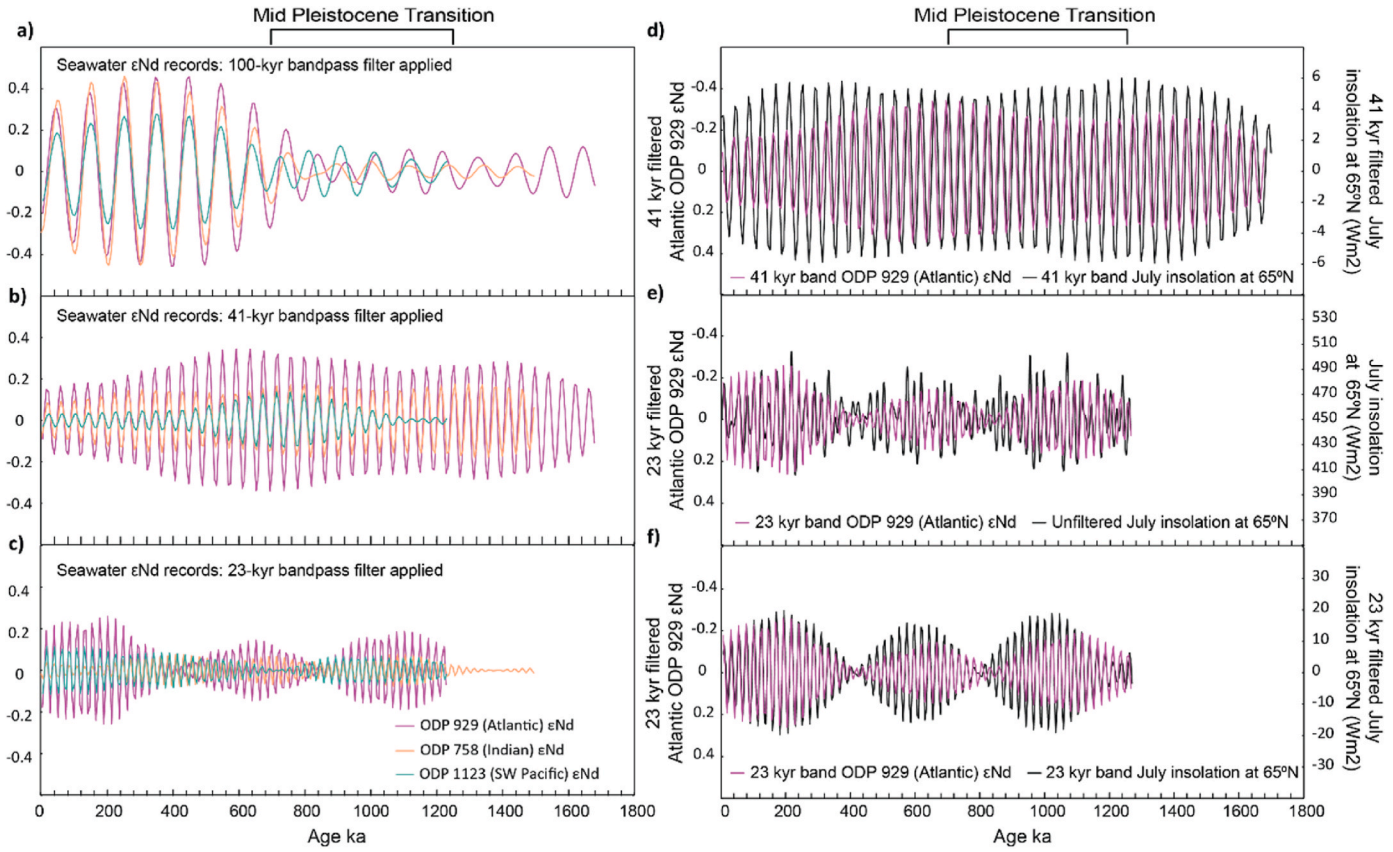

Fig. 4. Bandpass filtered seawater ε_{Nd} and insolation records. (a–c): Reconstructed seawater ε_{Nd} from the Atlantic (ODP Site 929), Indian (ODP Site 758) and SW Pacific (ODP Site 1123) with 100 kyr (a), 41 kyr (b) and 23 kyr (c) bandpass filters applied. Orbital-scale variability between records is largely in-phase, with the notable exception of the weak 100 kyr cyclicity during the middle to late Mid-Pleistocene Transition (MPT). **(d–f):** Atlantic (ODP Site 929) seawater ε_{Nd} variability is clearly in phase with July insolation at 65°N, predicted to be a key control on the build-up and decay of northern hemisphere ice sheets according to the Milankovitch theory of ice ages. This suggests a northern hemisphere climatic control on seawater ε_{Nd} cycles across the last 1800 kyr. Bandpass filter applied using Acycle v 2.4.1 (Li et al., 2019).

largely in-phase, suggesting a common global driver (Fig. 4a–c).

To investigate the drivers of global ε_{Nd} variability, PCA was performed on the authigenic ε_{Nd} time series of ODP sites 929 (Atlantic), 758 (Indian) and 1123 (SW Pacific) (Fig. 2, see Subsection 2.3. for details). The dominant mode of variability (PC1) explains 68% of total ε_{Nd} variance and is strongly correlated with the deep equatorial Atlantic ε_{Nd} reconstruction of ODP Site 929 ($r^2 = 0.85$, see Fig. S4). This strong correlation suggests Atlantic ε_{Nd} can explain the majority of variance within PC1, and thus exerts a strong control on global seawater ε_{Nd} variability. The correlation between PC1 and individual records decreases along the pathway of the thermohaline circulation, away from the Atlantic, with lower correlations within the equatorial Indian ($r^2 = 0.61$) and SW Pacific ($r^2 = 0.41$) oceans (Fig. S4). The pattern of global seawater ε_{Nd} across the middle to late Quaternary therefore appears to be driven by changes in the Atlantic, where deep water ε_{Nd} was more positive during glacial periods, and more negative during interglacials. This variability propagated through the global thermohaline circulation system from the Atlantic to the Indian and SW Pacific oceans. The attenuated amplitude of glacial-interglacial ε_{Nd} variability within the Indian and SW Pacific oceans compared with the Atlantic reflects mixing of NSW with voluminous Pacific- and Southern Ocean-sourced deep waters (Fig. 2b).

A strong correlation exists between modelled northern hemisphere ice volume (Köhler and van de Wal, 2020) and both Atlantic seawater ε_{Nd} ($r^2 = 0.58$) and ε_{Nd} PC1 ($r^2 = 0.65$) (Fig. S5). Obliquity (41 kyr) bandpass filtered Atlantic ε_{Nd} is also strongly correlated with both modelled northern hemisphere ice volume (Köhler and van de Wal, 2020) and 41 kyr bandpass filtered summer (July) insolation at 65°N, which it lags by several thousand years (Fig. 4d; $r^2 = 0.94$ when a lag of 6 kyr between ε_{Nd} and insolation is applied). Summer insolation at 65°N is thought to be a particularly important driver of northern hemisphere ice sheet waxing and waning, and thus a key metric determining global ice volume (Milankovitch, 1941; Hays et al., 1976). The timing and relative strength of precessional (i.e. 18-23 kyr) Atlantic ε_{Nd} cycles is also in phase with July insolation at 65°N ($r^2 = 0.72$), which itself is strongly driven by the precessional cycle of Earth's orbit (Hays et al., 1976) (Fig. 4e–f). All these observations indicate that Atlantic seawater ε_{Nd} variability was primarily driven by northern hemisphere climate throughout the last 1700 kyr. Given the control that Atlantic seawater ε_{Nd} exerts on Indian and SW Pacific Ocean ε_{Nd}, it is evident that global seawater ε_{Nd} variability was driven by fluctuations in northern hemisphere climate, which in turn were apparently driven by insolation changes.

A lag of several thousand years between insolation forcing and response, as observed between 41-kyr filtered authigenic ε_{Nd} and obliquity 41-kyr filtered northern hemisphere insolation, is the order of time required for the build-up and decay of ice sheets (Dalton et al., 2022). This relationship suggests Atlantic ε_{Nd} variability may reflect changes in Nd input to the North Atlantic region, driven by the waxing and waning of northern hemisphere ice sheets. This driver has been hypothesized to control changes in NSW ε_{Nd} during the last glacial cycle (Pöppelmeier et al., 2020b; Pöppelmeier et al., 2021; Zhao et al., 2019), when ε_{Nd} values in the deep North Atlantic shifted to ~ -11, more positive than today's value of ~ -13 (see Subsection 3.2.). A plausible alternative explanation for more positive authigenic ε_{Nd} values during glacials may be a greater contribution of bottom waters sourced in the

Nordic Seas to NSW, which today exhibit more radiogenic ε_{Nd} values (~-8.3, Fig. 1) (Lambelet et al., 2016; van de Flierdt et al., 2016). However, this is inconsistent with observations from the last glacial period, which indicate ε_{Nd} values in the Nordic Seas were actually less radiogenic during the last glacial period (ε_{Nd} of between −12.2 and −12.8, Struve et al., 2019).

3.3. Atlantic Meridional Overturning Circulation (AMOC) across the '900 ka event'

A leading hypothesis to explain the MPT invokes an AMOC perturbation across the interglacial-glacial cycle of MIS 23–22 (917–866 ka) (Elderfield et al., 2012; Pena and Goldstein, 2014; Tachikawa et al., 2021), coinciding with a period of global cooling and a step-like expansion in ice volume known as the '900 ka event' (Clark et al., 2006; Elderfield et al., 2012). This hypothesis posits i) a dramatic shoaling of NCW within the Atlantic, leading to a greatly expanded lower circulation cell comprised of carbon-rich Southern Ocean sourced waters (SSW), and ii) a much weaker AMOC (Pena and Goldstein, 2014). The combined effects of these circulation changes were thought to result in a 'thermohaline circulation crisis', spanning MIS 24–22 and incorporating the relatively cold interglacial MIS 23 (Pena and Goldstein, 2014). This crisis in turn sustained a cool northern hemisphere climate and glacial-like conditions throughout MIS 24–22 (936–866 ka) (Elderfield et al., 2012). During MIS 22, reconstructed seawater ε_{Nd} within the Atlantic shifted towards more positive values (−9.4 at ODP 929) than observed during previous glacial periods (Kim et al., 2021; Pena and Goldstein, 2014; Tachikawa et al., 2021) (ODP 929 average glacial maximum ε_{Nd} is −11.0 from 1700–900 ka - Fig. 2 and Fig. S6). More positive Atlantic seawater ε_{Nd} values are also observed during each subsequent glacial maximum following MIS 22 (ODP 929 average glacial maximum ε_{Nd} is −9.8 from 900–6 ka).

The more positive Atlantic ε_{Nd} values during MIS 23-22 have previously been interpreted to reflect an SSW expansion in response to this 'thermohaline circulation crisis', which then re-occurred during subsequent glacial periods, including the Last Glacial Maximum (LGM; 24–18 ka) (Kim et al., 2021; Pena and Goldstein, 2014; Tachikawa et al., 2021). However, we now know that the ε_{Nd} composition of NSW varied in the past, with a shift towards more positive values during periods of northern hemisphere glaciation (Pöppelmeier et al., 2020a; Pöppelmeier et al., 2021; Zhao et al., 2019). For example, seawater ε_{Nd} reconstructions from a North Atlantic (30–40°N) depth transect of sediment cores spanning 1800–5000 m water depth revealed that ε_{Nd} had shifted towards more positive values throughout the water column during the LGM (Fig. S2) (Zhao et al., 2019). These ε_{Nd} data, along with earth system model runs, indicate that the basin-wide positive shift in Atlantic seawater ε_{Nd} during the last glacial cycle can largely be explained by a change in the ε_{Nd} of NSW itself, with a smaller northward expansion of SSW than previously thought (Pöppelmeier et al., 2020b; 2021, 2022; Zhao et al., 2019).

The increase in NSW ε_{Nd} values during the last glacial cycle is thought to be a direct consequence of the climatic conditions during that time (Pöppelmeier et al., 2022; Zhao et al., 2019). A cooler climate and the presence of large northern hemisphere ice sheets, especially the Laurentide Ice Sheet, acted to reduce inputs of both dissolved and detrital Nd with very low ε_{Nd} values into the North Atlantic, leading to a more positive NSW ε_{Nd}. This is consistent with model data indicating a ~67% reduction in both high northern latitude river discharge and weathering rates during past glaciations (von Blanckenburg et al., 2015). Given the close link between northern hemisphere climate indices and Atlantic authigenic ε_{Nd} data that we observe since 1700 ka (Subsection 3.1., Fig. 4 and Fig. S5), we investigate whether a similar change in NSW ε_{Nd} could also explain the changes in Atlantic seawater ε_{Nd} recorded during MIS 23–22.

A depth transect of ε_{Nd} records from North Atlantic sediment cores shows that IODP Site U1313 was bathed in NSW throughout the last glacial cycle (Pöppelmeier et al., 2021), and can thus be used as an approximation for the NSW endmember during that time interval (Fig. S2). The last glacial period was characterized by the most severe glaciations effecting the circum-Atlantic region during the Late Quaternary, with the maximum extent of the North American and Eurasian ice sheets during the LGM being equivalent to – or greater than – that during MIS 23–22 (Batchelor et al., 2019; Köhler and van de Wal, 2020). Based on the observation that NSW continued to bathe IODP Site U1313 even during an extreme glaciation, such as the LGM (Pöppelmeier et al., 2021), we propose that IODP Site U1313 was bathed in NSW during other glacial periods of the Quaternary as well, and thus can be used as an approximation for past changes in NSW ε_{Nd}.

To assess the degree to which ε_{Nd} changes in the equatorial Atlantic (ODP 929), Indian (ODP 758) and SW Pacific (ODP 1123) can be attributed to changes in NSW ε_{Nd} rather than circulation changes, we apply a binary mixing model to these records (see Subsection 2.4). Any significant shoaling of NSW and expansion in SSW would manifest as a lower fraction of NSW reaching ODP sites 929, 758 and 1123 within this mixing model. Because Site 929 is located at the water mass boundary between northward flowing SSW and NSW, the effects of any major AMOC changes, especially a large SSW expansion, should be clearly observed at this site.

The mixing model shows no evidence for a significant disruption of the AMOC during MIS 23–22 (Fig. 5). Our mixing model instead suggests that the step-change in Atlantic ε_{Nd} towards more positive values during MIS 22 reflects a more positive NSW end member at this time, as seen in the authigenic ε_{Nd} record of IODP Site U1313 (Fig. 2), rather than a major expansion in SSW bathing ODP Site 929. We therefore propose that the change in NSW ε_{Nd} during MIS 22 was caused by a colder northern hemisphere climate and associated increase in northern hemisphere ice sheet volume, as has been argued to explain the more positive NSW ε_{Nd} during the last glacial cycle (Pöppelmeier et al., 2022; Zhao et al., 2019), rather than a major AMOC disruption (Pena and Goldstein, 2014; Howe et al., 2016).

The results of this mixing model, which suggest no significant incursions of SSW into the deep Atlantic during MIS 24–22, contradicts previous assessments of geochemical data from the late Pleistocene, particularly nutrient-based proxies, such as benthic foraminifera $\delta^{13}C$ (e.g. Raymo et al., 1990). Very negative Late Pleistocene $\delta^{13}C$ values in the deep Atlantic have long been interpreted as a shoaling of NSW and widespread incursions of SSW during glacial periods (Fig. 6a). This is exemplified by the LGM, when $\delta^{13}C$ data suggest widespread incursions of SSW into the deep Atlantic (e.g. Duplessy et al., 1988; Curry and Oppo, 2005; Gebbie, 2014; Peterson et al., 2014), coupled with a weakened AMOC (Muglia et al., 2018). However, recent studies incorporating multiple circulation tracers suggest northward incursions of SSW during the last glacial cycle were less severe than previously thought (Gebbie, 2014; Pöppelmeier et al., 2020a), with substantial AMOC weakening limited to the LGM – as observed in our mixing model (Fig. 5) – or periods of intense freshwater input to the North Atlantic (e.g. during Heinrich stadials, Böhm et al., 2015). The extremely negative $\delta^{13}C$ values in the deep Atlantic during the last glacial cycle likely instead reflect reduced air-sea exchange during bottom water formation and increased remineralization of ^{13}C-depleted organic carbon, alongside more modest circulation changes (e.g. Gebbie, 2014; Muglia et al., 2018).

A global shift in deep ocean $\delta^{13}C$ toward lower values is also observed across MIS 24–22, during the so-called '900 ka event' (Fig. 6a) (Raymo et al., 1997). At DSDP Site 607 in the North Atlantic (subsequently re-occupied as IODP Site U1313, Fig. 1), $\delta^{13}C$ values reach −1.1‰ during MIS 24 (918 ka), as negative as those in the deep equatorial eastern Pacific (ODP 846, -1.1‰; see Fig. 6). This represents a breakdown in the Pacific-Atlantic $\delta^{13}C$ gradient, whereby the deep Pacific has more negative $\delta^{13}C$ values than the Atlantic, owing to larger amounts of remineralised, ^{12}C-rich organic carbon. This gradient has existed throughout most of the Plio-Pleistocene, and its breakdown has

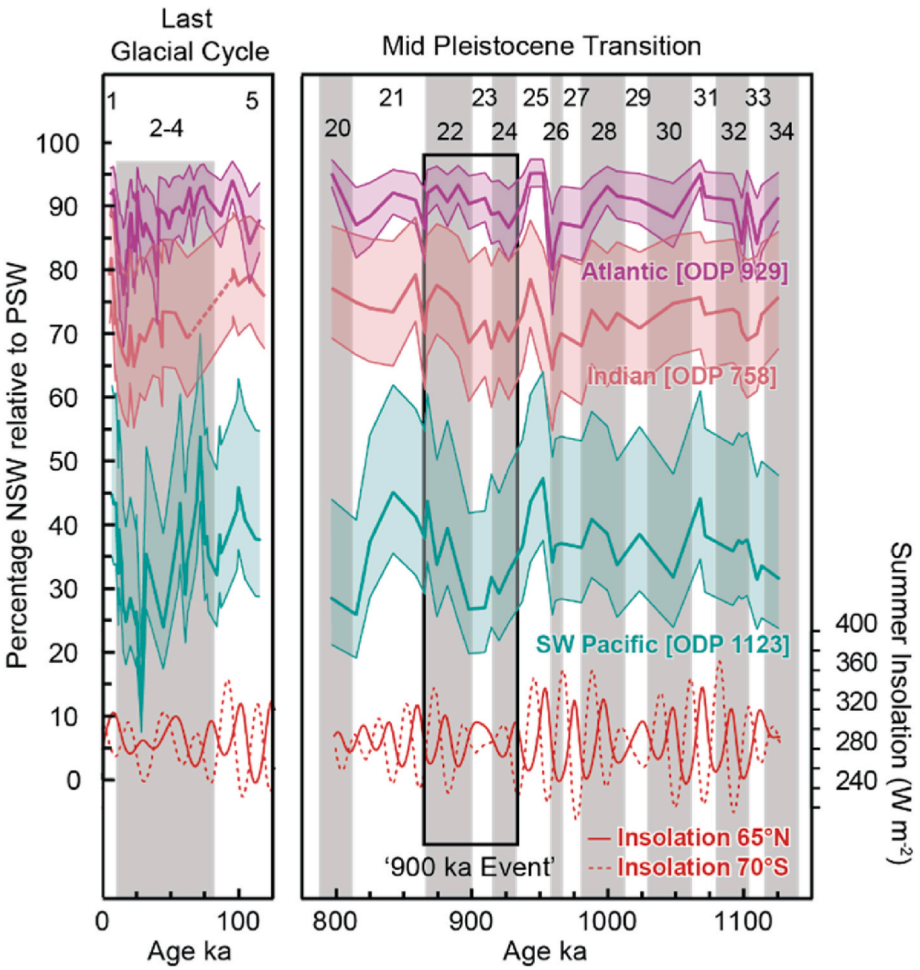

Fig. 5. Results of a binary mixing calculation, showing percentage of Northern sourced waters (NSW) relative to Pacific sourced waters bathing core sites, alongside summer insolation. The deep North Atlantic composite ε_{Nd} record of IODP Site U1313/V30-97/DSDP Site 607 (Fig. 2) is assumed to reflect ε_{Nd} of NSW and is thus used to constrain the Atlantic end-member. There is no evidence for a substantial disruption in the Atlantic Meridional Overturning Circulation (AMOC) during the '900 ka event' (i.e. reduced %NSW). A decrease in NSW advection to the SW Pacific (ODP Site 1123) occurs during interglacial MIS 23, coincident with prolonged low summer insolation at 70°S. Uncertainty envelopes calculated by varying Nd concentrations [Nd] in Atlantic sourced water by ± 50%. Numbers at the top of the figure correspond to MIS, with grey shading denoting glacial periods.

been interpreted as reflecting widespread incursions of SSW into the deep North Atlantic during both MIS 24 and 22 (Raymo et al., 1990), becoming a feature of subsequent glacial periods. However, this interpretation requires almost pure SSW or PDW bathing core sites within the North Atlantic, something not supported by the negative authigenic ε_{Nd} values across MIS 24-22 measured at Site U1313/607 ($\varepsilon_{Nd} = -12.3$ to -10.8), which at no time reach values observed within the deep South Atlantic (ODP Site 1090, $\varepsilon_{Nd} = -8.0$ to -7.4 across MIS 24–22, Fig. 6b) (Pena and Goldstein, 2014) or deep Pacific ($\varepsilon_{Nd} = -4$). A gradient in authigenic ε_{Nd} is observed from the deep North Atlantic to the South Atlantic throughout the MPT, reflecting continued southward advection of NSW, which mixed with SSW along its flow path. A north-south gradient is also observed in nutrient reconstructions from the deep Atlantic during the MPT, reflecting continued ventilation of Site U1313/607 by North Atlantic sourced waters (Farmer et al., 2019).

The discrepancy between δ^{13}C-based interpretations of expanded SSW into the deep Atlantic, and the authigenic ε_{Nd}-based mixing model presented here suggesting little to no significant change in AMOC across the '900 ka event' of MIS 24–22, could result from several factors. It may be that – as with the LGM – there was a moderate increase in SSW penetration into the North Atlantic, causing more radiogenic ε_{Nd} bottom waters at IODP Site U1313. However, authigenic ε_{Nd} data rule out the presence of almost pure PDW and/or SSW within the Atlantic required to explain such negative North Atlantic δ^{13}C values purely via circulation changes. The observed δ^{13}C decrease in the Atlantic may alternatively reflect (i) a change in deep ocean δ^{13}C inventories due to increased weathering of ^{12}C-rich organic carbon, perhaps due to exposure of continental margins as sea levels dropped or increased terrestrial carbon inputs due to greater aridity; (ii) changing bottom water formation mechanisms within the North Atlantic, Nordic Seas, or Labrador Sea, leading to reduced air-sea gas exchange (Raymo et al., 2004); (iii) greater ageing of North Atlantic bottom waters, leading to increased nutrient content and lower δ^{13}C values (Farmer et al., 2019). Regardless, the Atlantic ε_{Nd} records (Fig. 2) and the mixing model (Fig. 5) presented here argue against a significant weakening or 'collapse' of the AMOC at this time.

3.4. Southern Ocean circulation reorganization across the '900 ka event'

Despite showing no clear evidence for a substantial change in Atlantic circulation during the '900 ka event', the ε_{Nd} record of ODP 1123 and the mixing model presented in Subsection 3.3 indicate reductions in NSW in the SW Pacific during the weak interglacial MIS 23 (Subsection 3.2, Fig. 5). Given the lack of clear evidence for a decrease in NSW reaching the deep equatorial Atlantic, the reduction in NSW propagation into the SW Pacific during MIS 23 suggests circulation

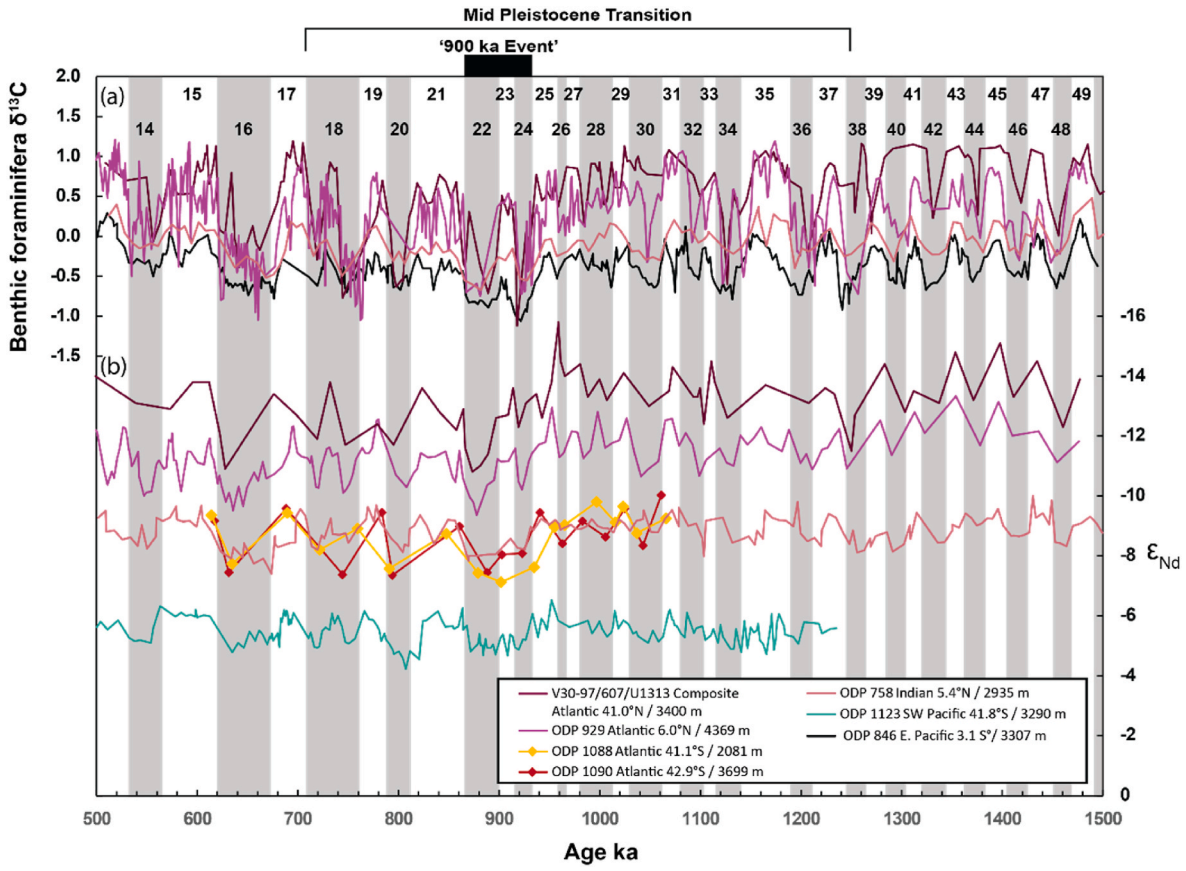

Fig. 6. Comparison between (**a**) $\delta^{13}C$ and (**b**) authigenic ε_{Nd} records from the Atlantic spanning the MPT. ε_{Nd} data suggest the extremely negative $\delta^{13}C$ during MIS 24–22, previously interpreted as reflecting widespread SSW incursions throughout the deep Atlantic, cannot be purely explained by water mass mixing.

changes within the Southern Ocean.

Reconstructions of sea surface temperature (Becquey and Gersonde, 2002; Martínez-Garcia et al., 2009; An et al., 2024) and paleo-productivity (Kaiser et al., 2021), along with microfossil abundance data (Marcks et al., 2023), indicate that cold, glacial-like climatic conditions persisted throughout much of the Southern Ocean during MIS 24–22 (Starr et al., 2021; Clark et al., 2024). This prolonged cold interval likely resulted from southern hemisphere insolation during MIS 23, which was anomalously low for an interglacial (Fig. 5) (Elderfield et al., 2012). It has been demonstrated that periods of atmospheric cooling over the Southern Ocean during the late Quaternary led to more sea-ice formation around Antarctica (Jansen, 2017). Increased sea-ice formation and associated brine rejection can lead to salinification of Southern Ocean shelf waters and ultimately densification of AABW, instigating a salinity-driven stratification of the Southern Ocean interior in response to atmospheric cooling (Jansen, 2017). Such a stratification could explain the reduced NSW propagation into the deep SW Pacific, by limiting mixing of NSW into lower CDW, which baths ODP Site 1123 today. The same reduction in NSW is not clearly observed at Indian Ocean site ODP 758 (Fig. 5), suggesting continued admixture of NSW into upper CDW, which went on to bath the core site. This was also the case during the last glacial cycle, when ε_{Nd} data suggest a water mass boundary developed separating relatively NSW-rich waters bathing ODP Site 758 (2935 m water depth) and NSW-poor waters bathing equatorial Indian Ocean site SK129-CR2 (3800 m water depth) (Piotrowski et al., 2009; Wilson et al., 2015) (Fig. S7).

Deep ocean stratification of the Southern Ocean interior, as suggested by our authigenic ε_{Nd} data, combined with reduced air-sea gas exchange due to more extensive and thicker sea ice, has the potential to cause a reduction in atmospheric CO_2 of up to 40 ppm (Gildor and Tziperman, 2001; Lear et al., 2016; Marzocchi and Jansen, 2019). A CO_2 decrease in response to expanded Antarctic sea ice could, in turn, lead to an expansion in northern hemisphere ice sheets across MIS 24–22. This climate feedback is thought to have played a role in glacial intensification during the early stages of the last glacial cycle, and may play an important role in the initiation of late Quaternary glaciations (Hasenfratz et al., 2019; Marzocchi and Jansen, 2019; Williams et al., 2021). This feedback provides a plausible explanation for the expansion of global ice volume across MIS 24–22, and the lengthening of glacial periods, which is a hallmark of the MPT. However, it fails to explain why previous intervals of cooling failed to illicit a similar response. It therefore appears changes in other aspects of the climate system were also required to explain the onset of the MPT. One such change may have been northern hemisphere regolith removal, which we discuss in more detail in the following Subsection 3.5.

3.5. *Atlantic ε_{Nd} suggests regolith removal preceded the mid-pleistocene transition*

Immediately preceding the MPT, between ca. 1450–1250 ka (largely coinciding with MIS 47–39), glacial and interglacial seawater ε_{Nd} values at Atlantic sites ODP 929 and IODP U1313 were significantly more negative (−11.36 to −13.3 at ODP 929) than after the MPT (−9.4 to −12 at ODP 929) (Fig. 2). Prior to 1450 ka, Atlantic ε_{Nd} fell approximately within the range of post-MPT glacial-interglacial variability (−10.1 to −12.2 at ODP 929). The interval from 1450–1250 ka was apparently the first time, when Atlantic authigenic ε_{Nd} values reached such minima since at least 4 Ma (Fig. S8). We interpret these Atlantic seawater ε_{Nd} minima as results of increased Nd input from the rocks of the North American Shield, which have characteristically negative ε_{Nd} values, into the formation regions of NSW and its precursor water masses (Fig. 1). The period of particularly negative NSW ε_{Nd} values lasted until

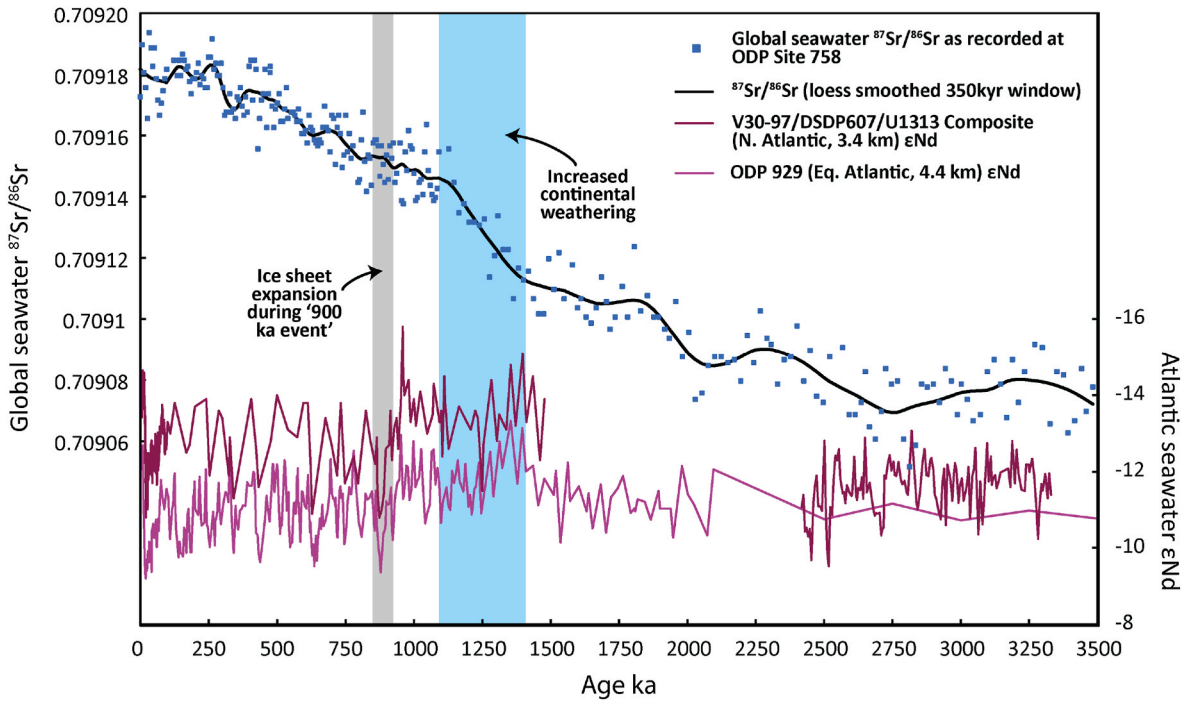

Fig. 7. Plio-/Pleistocene evolution of global seawater $^{87}Sr/^{86}Sr$ (Farrell et al., 1995) and Atlantic seawater ε_{Nd} (Howe and Piotrowski, 2017; Kim et al., 2021; Lang et al., 2016; Lippold et al., 2016; Pöppelmeier et al., 2021, 2018; this study). Between approximately 1.4 and 1.1 Ma, the rate of change in seawater $^{87}Sr/^{86}Sr$ ratios increased markedly (blue shading), coinciding with shifts in Atlantic ε_{Nd} values towards more negative values during interglacials. We attribute these changes to unroofing and weathering of basement rocks of the North American Shield. Together, these data suggest the removal of substantial North American regolith occurred at least 500,000 years prior to the expansion in ice volume at ~900 ka (grey shading).

approximately 1250 ka, coinciding with the onset of a long-term increase in maximum global ice volume at the start of the MPT (Elderfield et al., 2012; Köhler and van de Wal, 2020; Miller et al., 2020), thought to reflect northern hemisphere ice sheet expansion (An et al., 2024). A second interval of particularly negative Atlantic seawater ε_{Nd} values occurred during the MPT, between 1050 ka and 950 ka (MIS 32–25: ε_{Nd} values of −11.3 to −13 at ODP 929), immediately prior to the circulation changes discussed in Subsection 3.4 and subsequent step-like expansion in ice volume during MIS 22 (Elderfield et al., 2012; Köhler and van de Wal, 2020; Miller et al., 2020; An et al., 2024) (Fig. 2). The first of these negative Atlantic ε_{Nd} excursions coincided with a sharp increase in the $^{87}Sr/^{86}Sr$ ratio of global seawater (Farrell et al., 1995) (Fig. 7), which reflects increased weathering of silicate rocks and has been linked to an increased erosion of basement rocks of the North American Shield (Roy et al., 2004; Yehudai et al., 2021). These negative ε_{Nd} excursions also coincide with a shift in detrital ε_{Nd} of Arctic Ocean sediments toward more negative values, equally interpreted as a result of increased erosion of basement rocks of the North American Shield (Muratli et al., 2022) (Fig. S9).

The increased erosion of basement rocks of the North American Shield, as evidenced by shifts in both seawater Sr and Nd isotopes and detrital Nd isotopes between 1450–1250 ka (MIS 47–39), was followed by an ice-sheet expansion from 936–866 ka (MIS 24–22), as reflected in sea level reconstructions (Fig. 2 and S8). This is, in general, consistent with the regolith hypothesis for the initiation of the MPT, which proposes that the removal of a low-friction regolith layer and increased exposure of high-friction crystalline basement rocks are a prerequisite for the build-up of larger and/or thicker North American ice sheets (Clark and Pollard, 1998). These ice sheets were more resilient to deglaciation, leading to longer glacial-interglacial cycles averaging ~100 kyr (Köhler and van de Wal, 2020).

The Atlantic ε_{Nd} data presented here suggest that the onset of intense erosion and weathering of crystalline basement rocks had begun by at least ~1435 ka (MIS 47), predating the onset of the MPT by approximately 200,000 years (Clark et al., 2006) and the hypothesized expansion of ice sheets across MIS 24-22 by ~500,000 years (Elderfield et al., 2012; Rohling et al., 2014; Ford et al., 2019; Miller et al., 2020; Köhler and van de Wal, 2020; An et al., 2024). It therefore appears that, while removal of a regolith 'blanket' from the North American continent may be a pre-requisite for the ice volume increase across the MPT, other climate feedback(s) were then required to initiate the longer, ~100 kyr climate cycles of the late Quaternary (Clark and Pollard, 1998). The new authigenic ε_{Nd} data presented in this study suggest one such feedback may have been the reorganization of Southern Ocean circulation, possibly linked to Antarctic sea-ice expansion around the time of the '900 ka event' (see Subsection 3.4).

4. Conclusions

The three new deep ocean authigenic ε_{Nd} records presented here show pronounced orbital-scale variability over the last 1700 kyr. This variability was driven by changes in North Atlantic ε_{Nd}, which subsequently propagated throughout much of the global circulation system. The authigenic ε_{Nd} values recorded in the North Atlantic, equatorial Indian and SW Pacific oceans varied in concert, suggesting that the global thermohaline circulation was effective in propagating northern Atlantic-sourced waters through the Atlantic and Southern oceans, although this was at times diminished, especially during glacial periods following the MPT. When combined in a mixing model utilizing the previously published composite authigenic ε_{Nd} record from the North Atlantic IODP Site U1313 (Kim et al., 2021; Lang et al., 2016; Lippold et al., 2016; Pöppelmeier et al., 2018, 2021), these data provide no clear evidence for a substantial AMOC 'crisis' during MIS 24–22 (Pena and Goldstein (2014) (Fig. 5). Our results do indicate a reduction in NSW flow into the deep SW Pacific during weak interglacial MIS 23. This points to a reorganization of Southern Ocean circulation during MIS 23,

which we link to southern hemispheric cooling and associated sea-ice expansion that began during glacial MIS 24. We hypothesize this reorganization of Southern Ocean circulation lowered atmospheric CO_2, suppressing global temperatures and priming the climate system for northern hemisphere ice sheet expansion during glacial MIS 22.

Prior to the MPT, between 1450–1250 k, a prolonged interval of relatively negative NSW ε_{Nd} values documents increased weathering and erosion of basement rocks of the North American Shield around the North Atlantic. The timing of this prolonged weathering interval roughly 200,000 years prior to the MPT and 500,000 years before major northern hemisphere ice sheet expansion suggests that, while removal of a northern hemisphere regolith layer may well have been a pre-requisite for ice sheet expansion across the MPT, other triggers were likely required to cause the build-up of larger ice sheets across the MPT. Our ε_{Nd} data indicate that one such trigger may be a reorganization of Southern Ocean circulation during MIS 24–22.

CRediT authorship contribution statement

Thomas J. Williams: Conceptualization, Methodology, Formal analysis, Writing – original draft, Writing – review & editing, Visualization, Project administration. **Alexander M. Piotrowski:** Conceptualization, Methodology, Writing – original draft, Writing – review & editing, Supervision, Project administration, Funding acquisition. **Jacob N.W. Howe:** Conceptualization, Methodology, Writing – original draft, Funding acquisition. **Claus-Dieter Hillenbrand:** Conceptualization, Writing – original draft, Writing – review & editing, Supervision, Project administration, Funding acquisition. **Claire S. Allen:** Conceptualization, Writing – original draft, Writing – review & editing, Supervision. **Josephine A. Clegg:** Methodology.

Declaration of competing interest

The authors declare that they have no known competing financial interests or personal relationships that could have appeared to influence the work reported in this paper.

Acknowledgements

Samples for this work were supplied by the International Ocean Discovery Program (IODP). V. Rennie is thanked for help with picking and analysing foraminifera samples from ODP 1123. V. Rennie, S. Misra, J. Day, E. Tipper and H. Chapman are all thanked for providing technical assistance. Funding for this research was provided by NERC grants NE/K005235/1 and NE/F006047/1 to A.M.P. T.J.W. was supported by a UK Natural Environment Research Council (NERC) Algorithm PhD studentship, and J.N.W.H. was supported by a Rutherford Memorial Scholarship. C-D.H. and C.S.A are supported by NERC. This research was partially supported by the Australian Research Council Special Research Initiative, Australian Centre for Excellence in Antarctic Science (Project Number SR200100008). Principal Component Analysis was performed using MATLABs PCA function. We thank E.E. Martin for thoughts on an early version of the manuscript, and Maayan Yehudai and an anonymous referee for their constructive reviews.

Appendix A. Supplementary data

Supplementary data to this article can be found online at https://doi.org/10.1016/j.quascirev.2024.109055.

Data availability

All data is included in the manuscript and supplementary materials. Data will also be made available on the website Pangea.de

References

Abbott, A.N., Haley, B.A., McManus, J., Reimers, C.E., 2015a. The sedimentary flux of dissolved rare earth elements to the ocean. Geochim Cosmochim Acta 154, 186–200. https://doi.org/10.1016/j.gca.2015.01.010.

Abbott, A.N., Haley, B.A., McManus, J., 2015b. Bottoms up: sedimentary control of the deep North Pacific Ocean's ε_{Nd} signature. Geology 43, 1035. https://doi.org/10.1130/G37114.1.

Abbott, A.N., Löhr, S.C., Payne, A., Kumar, H., Du, J., 2022. Widespread lithogenic control of marine authigenic neodymium isotope records? Implications for paleoceanographic reconstructions. Geochim Cosmochim Acta 319, 318–336. https://doi.org/10.1016/j.gca.2021.11.021.

Amakawa, H., Sasaki, K., Ebihara, M., 2009. Nd isotopic composition in the central North Pacific. Geochim Cosmochim Acta 73, 4705–4719. https://doi.org/10.1016/j.gca.2009.05.058.

An, Z., Zhou, W., Zhang, Z., Zhang, X., Liu, Z., Sun, Y., Clemens, S.C., Wu, L., Zhao, J., Shi, Z., Ma, X., Yan, H., Li, G., Cai, Y., Yu, J., Sun, Y., Li, S., Zhang, Y., Stepanek, C., Lohmann, G., Dong, G., Cheng, H., Liu, Y., Jin, Z., Li, T., Hao, Y., Lei, J., Cai, W., 2024. Mid-Pleistocene climate transition triggered by Antarctic Ice Sheet growth. Science 385, 560–565. https://doi.org/10.1126/science.abn4861.

Barker, S., Zhang, X., Jonkers, L., Lordsmith, S., Conn, S., Knorr, G., 2021. Strengthening atlantic inflow across the mid-pleistocene transition. Paleoceanogr. Paleoclimatol. 36, e2020PA004200. https://doi.org/10.1029/2020PA004200.

Barker, S., Starr, A., van der Lubbe, J., Doughty, A., Knorr, G., Conn, S., Lordsmith, S., Owen, L., Nederbragt, A., Hemming, S., Hall, I., Levay, L., IODP EXP 361 Shipboard Science Party, 2022. Persistent influence of precession on northern ice sheet variability since the early Pleistocene. Science 376, 961–967. https://doi.org/10.1126/science.abm4033.

Batchelor, C.L., Margold, M., Krapp, M., Murton, D.K., Dalton, A.S., Gibbard, P.L., Stokes, C.R., Murton, J.B., Manica, A., 2019. The configuration of Northern Hemisphere ice sheets through the Quaternary. Nat. Commun. 10, 1–10. https://doi.org/10.1038/s41467-019-11601-2.

Becquey, S., Gersonde, R., 2002. Past hydrographic and climatic changes in the subantarctic zone of the South Atlantic - the Pleistocene record from ODP site 1090. Palaeogeogr. Palaeoclimatol. Palaeoecol. 182, 221–239. https://doi.org/10.1016/S0031-0182(01)00497-7.

Behrens, M.K., Pahnke, K., Schnetger, B., Brumsack, H.-J., 2018. Sources and processes affecting the distribution of dissolved Nd isotopes and concentrations in the West Pacific. Geochim Cosmochim Acta 222, 508–534. https://doi.org/10.1016/j.gca.2017.11.008.

Berends, C.J., Köhler, P., Lourens, L.J., van de Wal, R.S.W., 2021. On the cause of the mid-pleistocene transition. Rev. Geophys. 59. https://doi.org/10.1029/2020RG000727.

Bickert, T., Curry, W., Wefer, G., 1997. Late Pliocene to Holocene (2.6-0 Ma) western equatorial Atlantic deep-water circulation: inferences from benthic stable isotopes. Proc. Ocean Drill. Progr. Sci. Results 154, 239–254.

Blaser, P., Lippold, J., Gutjahr, M., Frank, N., Link, J.M., Frank, M., 2016. Extracting foraminiferal seawater Nd isotope signatures from bulk deep sea sediment by chemical leaching. Chem. Geol. 439, 189–204. https://doi.org/10.1016/j.chemgeo.2016.06.024.

Blaser, P., Pöppelmeier, F., Schulz, H., Gutjahr, M., Frank, M., Lippold, J., Heinrich, H., Link, J.M., Hoffmann, J., Szidat, S., Frank, N., 2019. The resilience and sensitivity of Northeast Atlantic deep water εNd to overprinting by detrital fluxes over the past 30,000 years. Geochim Cosmochim Acta 245, 79–97. https://doi.org/10.1016/j.gca.2018.10.018.

Blaser, P., Gutjahr, M., Pöppelmeier, F., Frank, M., Kaboth-Bahr, S., Lippold, J., 2020. Labrador Sea bottom water provenance and REE exchange during the past 35,000 years. Earth Planet Sci. Lett. 542. https://doi.org/10.1016/j.epsl.2020.116299.

Böhm, E., Lippold, J., Gutjahr, M., Frank, M., Blaser, P., Antz, B., Fohlmeister, J, Frank, N., Andersen, M.B., Deininger, M., 2015. Strong and deep Atlantic meridional overturning circulation during the last glacial cycle. Nature 517, 73–76. https://doi.org/10.1038/nature14059.

Burton, K.W., Vance, D., 2000. Glacial-interglacial variations in the neodymium isotope composition of seawater in the Bay of Bengal recorded by planktonic foraminifera. Earth Planet Sci. Lett. 176, 425–441. https://doi.org/10.1016/S0012-821X(00)00011-X.

Chalk, T.B., Hain, M.P., Foster, G.L., Rohling, E.J., Sexton, P.F., Badger, M.P.S., Cherry, S. G., Hasenfratz, A.P., Haug, G.H., Jaccard, S.L., Martínez-García, A., Pälike, H., Pancost, R.D., Wilson, P.A., 2017. Causes of ice age intensification across the Mid-Pleistocene Transition. In: Proceedings of the National Academy of Sciences 201702143. https://doi.org/10.1073/pnas.1702143114.

Chen, J., Farrell, J.W., Murray, D.W., Prell, W.L., 1995. Timescale and paleoceanographic implications of a 3.6 m.y. oxygen isotope record from the northeast Indian Ocean (Ocean Drilling Program Site 758). Paleoceanography 10, 21–47. https://doi.org/10.1029/94PA02290.

Clark, P.U., Pollard, D., 1998. Origin of the middle Pleistocene transition by ice sheet erosion of regolith. Paleoceanography 13, 1–9. https://doi.org/10.1029/97PA02660.

Clark, P.U., Archer, D., Pollard, D., Blum, J.D., Rial, J.A., Brovkin, V., Mix, A.C., Pisias, N. G., Roy, M., 2006. The middle Pleistocene transition: characteristics, mechanisms, and implications for long-term changes in atmospheric pCO_2. Quat. Sci. Rev. 25, 3150–3184. https://doi.org/10.1016/j.quascirev.2006.07.008.

Clark, P.U., Shakun, J.D., Rosenthal, Y., Kohler, P., Bartlein, P.J., 2024. Global and regional temperature change over the past 4.5 million years. Science 383, 884–890. https://doi.org/10.1126/science.adi1908.

Curry, W.B., Oppo, D.W., 2005. Glacial water mass geometry and the distribution of $\delta^{13}C$ of ΣCO_2 in the western Atlantic Ocean. Paleoceanogr. Paleoclimatol. 20, PA1017. https://doi.org/10.1029/2004PA001021.

Curry, W.B., Shackleton, N.J., Richter, C., 1995. Proceedings of the ocean Drilling Program, 154 initial reports. Ocean Drilling Program, College Station, TX. https://doi.org/10.2973/odp.proc.ir.154.1995.

Dalton, A.S., Stokes, C.R., Batchelor, C.L., 2022. Evolution of the Laurentide and innuitian ice sheets prior to the last glacial maximum (115 ka to 25 ka). Earth Sci. Rev. 224, 103875. https://doi.org/10.1016/j.earscirev.2021.103875.

deMenocal, P., Archer, D., Leth, P., 1997. Pleistocene variations in deep Atlantic circulation and calcite burial between 1.2 and 0.6 Ma: a combined data-model approach. In: Proceedings of the Ocean Drilling Program, 154 Scientific Results. Ocean Drilling Program. https://doi.org/10.2973/odp.proc.sr.154.113.1997.

Du, J., Haley, B.A., Mix, A.C., 2020. Evolution of the global overturning circulation since the last glacial maximum based on marine authigenic neodymium isotopes. Quat. Sci. Rev. 241, 106396. https://doi.org/10.1016/j.quascirev.2020.106396.

Du, J., Haley, B.A., Mix, A.C., Abbott, A.N., McManus, J., Vance, D., 2022. Reactive-transport modeling of neodymium and its radiogenic isotope in deep-sea sediments: the roles of authigenesis, marine silicate weathering and reverse weathering. Earth Planet Sci. Lett. 596, 117792. https://doi.org/10.1016/j.epsl.2022.117792.

Duplessy, J.C., Shackleton, N.J., Fairbanks, R.G., Labeyrie, L., Oppo, D., Kallel, N., 1988. Deepwater Source Variations during the Last Climatic Cycle and Their Impact on the Global Deepwater Circulation. Paleoceanogr Paleoclimatol 3, pp. 343–360. https://doi.org/10.1029/PA003i003p00343.

Elderfield, H., Ferretti, P., Greaves, M., Crowhurst, S.J., McCave, I.N., Hodell, D.A., Piotrowski, A.M., 2012. Evolution of ocean temperature and ice volume through the mid-pleistocene climate transition. Science 337, 704–709. https://doi.org/10.1594/PANGAEA.786205, 1979.

Farmer, J.R., Hain, M.P., Sigman, D.M., Haug, G.H., Hesse, T., Muglia, J., 2019. Deep Atlantic Ocean carbon storage and the rise of 100,000-year glacial cycles. Nat. Geosci. 12 (5), 355–360. https://doi.org/10.1038/s41561-019-0334-6.

Farrell, J.W., Clemens, C., Gromet, L.P., 1995. Improved chronostratigraphic reference curve of late Neogene seawater $^{87}Sr/^{86}Sr$. Geology 23 (5), 403–406. https://doi.org/10.1130/0091-7613(1995)023<0403:ICRCOL>2.3.CO;2.

Filippova, A., Frank, M., Kienast, M., Rickli, J., Hathorne, E., Yashayaev, I.M., Pahnke, K., 2017. Water mass circulation and weathering inputs in the Labrador Sea based on coupled Hf–Nd isotope compositions and rare earth element distributions. Geochim Cosmochim Acta 199, 164–184. https://doi.org/10.1016/j.gca.2016.11.024.

Ford, H.L., Raymo, M.E., 2019. Regional and global signals in seawater δ18O records acrossthe mid-Pleistocene transition. Geology 48, 113–117. https://doi.org/10.1130/G46546.1.

Ganopolski, A., Calov, R., 2011. The role of orbital forcing, carbon dioxide and regolith in 100 kyr glacial cycles. Clim. Past 7, 1415–1425. https://doi.org/10.5194/cp-7-1415-2011.

Gebbie, J., 2014. How much did glacial North Atlantic water shoal? Paleoceanogr. Paleoclimatol. 29, 190–209. https://doi.org/10.1002/2013PA002557.

Gildor, H., Tziperman, E., 2001. A sea ice climate switch mechanism for the 100 kyr cycles. J. Geophys. Res. Oceans 106, 9117–9133.

Goldstein, S.J., Jacobs, S.B., 1987. The Nd and Sr isotopic systematics of river-water dissolved material: implications for the sources of Nd and Sr in seawater. Chem. Geol. 66, 245–272. https://doi.org/10.1016/0168-9622(87)90045-5.

Gourlan, A.T., Meynadier, L., Allègre, C.J., Tapponnier, P., Birck, J.-L., Joron, J.-L., 2010. Northern Hemisphere climate control of the Bengali rivers discharge during the past 4 Ma. Quat. Sci. Rev. 29, 2484–2498. https://doi.org/10.1016/j.quascirev.2010.05.003.

Griffithis, A., Lambelet, M., Crocket, K., Abell, R., Coles, B.J., Kreissig, K., Porter, D., Nitsche, F.O., Rehkämper, M., van de Flierdt, T., 2024. Neodymium isotope composition and rare earth element distribution of East Antarctic continental shelf and deep waters. Chem. Geol. 653, 122039. https://doi.org/10.1016/j.chemgeo.2024.122039.

Hasenfratz, A.P., Jaccard, S.L., Martinez-Garciia, A., Sigman, D.M., Hodell, D.A., Vance, D., Bernasconi, S.M., Kleiven, H.F., Haumann, F.A., Haug, G.H., 2019. The residence time of Southern Ocean surface waters and the 100,000-year ice age cycle. Science 363, 1080–1084. https://doi.org/10.1126/science.aat70.

Hays, J.D., Imbrie, J., Shackleton, N.J., 1976. Variations in the Earth's orbit: pacemaker of the ice ages. Science 194, 1121–1132. https://doi.org/10.1126/science.194.4270.1121.

Heaton, T.J., Köhler, P., Butzin, M., Bard, E., Reimer, R.W., Austin, W.E.N., Bronk Ramsey, C., Grootes, P.M., Hughen, K.A., Kromer, B., Reimer, P.J., Adkins, J., Burke, A., Cook, M.S., Olsen, J., Skinner, L.C., 2020. Marine20—the marine radiocarbon age calibration curve (0–55,000 cal BP). Radiocarbon 62, 779–820, 10.1017/RDC.2020.68.

Howe, J.N.W., Piotrowski, A.M., 2017. Atlantic deep water provenance decoupled from atmospheric CO_2 concentration during the lukewarm interglacials. Nat. Commun. 8. https://doi.org/10.1038/s41467-017-01939-w.

Howe, J.N.W., Piotrowski, A.M., Rennie, V.F., 2016. Abyssal origin for the early Holocene pulse of unradiogenic neodymium isotopes in Atlantic seawater. Geology 44 (10), 831–834. https://doi.org/10.1130/G38155.1.

Hu, R., Piotrowski, A.M., Bostock, H.C., Crowhurst, S., Rennie, V., 2016. Variability of neodymium isotopes associated with planktonic foraminifera in the Pacific Ocean during the Holocene and last glacial maximum. Earth Planet Sci. Lett. 447, 130–138. https://doi.org/10.1016/j.epsl.2016.05.011.

Jacobsen, S.B., Wasserburg, G.J., 1980. Sm-Nd isotopic evolution of chondrites. Earth Planet Sci. Lett. 50, 139–155. https://doi.org/10.1016/0012-821X(80)90125-9.

Jansen, M.F., 2017. Glacial Ocean Circulation and Stratification Explained by Reduced Atmospheric Temperature, vol. 114, pp. 45–50. https://doi.org/10.1073/pnas.1610438113.

Kaiser, E.A., Billups, K., Bradtmiller, L., 2021. A 1 million year record of biogenic silica in the Indian ocean sector of the Southern Ocean: regional versus global forcing of primary productivity. Paleoceanogr. Paleoclimatol. 36, 1–14. https://doi.org/10.1029/2020PA004033.

Kim, J., Goldstein, S.L., Pena, L.D., Jaume-Seguí, M., Knudson, K.P., Yehudai, M., Bolge, L., 2021. North atlantic deep water during Pleistocene interglacials and glacials. Quat. Sci. Rev. 269, 107146. https://doi.org/10.1016/j.quascirev.2021.107146.

Köhler, P., van de Wal, R.S.W., 2020. Interglacials of the Quaternary defined by northern hemispheric land ice distribution outside of Greenland. Nat. Commun. 11, 1–10. https://doi.org/10.1038/s41467-020-18897-5.

Lacan, F., Jeandel, C., 2005. Neodymium isotopes as a new tool for quantifying exchange fluxes at the continent-ocean interface. Earth Planet Sci. Lett. 232, 245–257. https://doi.org/10.1016/j.epsl.2005.01.004.

Lambelet, M., van de Flierdt, T., Crocket, K., Rehkämper, M., Kreissig, K., Coles, B., Rijkenberg, M.J.A., Gerringa, L.J.A., de Baar, H.J.W., Steinfeldt, R., 2016. Neodymium isotopic composition and concentration in the western North Atlantic Ocean: results from the GEOTRACES GA02 section. Geochim Cosmochim Acta 177, 1–29. https://doi.org/10.1016/j.gca.2015.12.019.

Lang, D.C., Bailey, I., Wilson, P.A., Chalk, T.B., Foster, G.L., Gutjahr, M., 2016. Incursions of southern-sourced water into the deep North Atlantic during late Pliocene glacial intensification. Nat. Geosci. 1–6. https://doi.org/10.1038/ngeo2688.

Lear, C.H., Billups, K., Rickaby, R.E.M., Diester-Haass, L., Mawbey, E.M., Sosdian, S.M., 2016. Breathing more deeply: deep ocean carbon storage during the mid-Pleistocene climate transition. Geology G38636. 1. https://doi.org/10.1130/G38636.1.

Li, M., Hinnov, L., Kump, L., 2019. Acycle: time-series analysis software for paleoclimate research and education. Comput. Geosci. 127, 12–22. https://doi.org/10.1016/j.cageo.2019.02.011.

Ling, H.F., Burton, K.W., O'Nions, R.K., Kamber, B.S., von Blanckenburg, F., Gibb, A.J., Hein, J.R., 1997. Evolution of Nd and Pb isotopes in Central Pacific seawater from ferromanganese crusts. Earth Planet Sci. Lett. 146, 1–12. https://doi.org/10.1016/S0012-821X(96)00224-5.

Lippold, J., Gutjahr, M., Blaser, P., Christner, E., Ferreira, M.L. de C., Mulitza, S., Christl, M., Wombacher, F., Böhm, E., Antz, B., Cartapanis, O., Vogel, H., Jaccard, S. L., 2016. Deep water provenience and dynamics of the (de)glacial Atlantic meridional overturning circulation. Earth Planet Sci. Lett. 445, 68–78. https://doi.org/10.1016/j.epsl.2016.04.013.

Lisiecki, L.E., Raymo, M.E., 2005. A Pliocene-Pleistocene stack of 57 globally distributed benthic 18O records. Paleoceanography 20, 1–17. https://doi.org/10.1029/2004PA001071.

Marcks, B.A., Dos Santos, T.P., Lessa, D.V.O., Cartagena-Sierra, A., Berke, M.A., Starr, A., Hall, I.R., Kelly, R.P., Robinson, R.S., 2023. Glacial Southern Ocean expansion recorded in foraminifera-bound nitrogen isotopes from the agulhas plateau during the mid-pleistocene transition. Paleoceanogr. Paleoclimatol. 38. https://doi.org/10.1029/2022pa004482.

Martínez-Garcia, A., Rosell-Melé, A., Geibert, W., Gersonde, R., Masqué, P., Gaspari, V., Barbante, C., 2009. Links between iron supply, marine productivity, sea surface temperature, and CO2 over the last 1.1 Ma. Paleoceanography 24, 1–14. https://doi.org/10.1029/2008PA001657.

Marzocchi, A., Jansen, M.F., 2019. Global cooling linked to increased glacial carbon storage via changes in Antarctic sea ice. Nat. Geosci. 12, 1001–1005. https://doi.org/10.1038/s41561-019-0466-8.

McKinley, C.C., Thomas, D.J., LeVay, L.J., Rolewicz, Z., 2019. Nd isotopic structure of the Pacific Ocean 40–10 Ma, and evidence for the reorganization of deep NorthNorth Pacific Ocean circulation between 36 and 25 Ma. Earth Planet Sci. Lett. 521, 139–149. https://doi.org/10.1016/j.epsl.2019.06.009.

Milankovitch, M., 1941. Canon of insolation and the ice-age problem. In: Kanon der Erdbestrahlung und seine Anwendung auf das Eiszeitenproblem) Belgrade, vol. 1941.

Miller, K.G., Browning, J.v., John Schmelz, W., Kopp, R.E., Mountain, G.S., Wright, J.D., 2020. Cenozoic sea-level and cryospheric evolution from deep-sea geochemical and continental margin records. Sci. Adv. 6. https://doi.org/10.1126/sciadv.aaz1346.

Muglia, J., Skinner, L.C., Schmittner, A., 2018. Weak overturning circulation and high Southern Ocean nutrient utilization maximized glacial ocean carbon. Earth Planet Sci. Lett. 496, 47–56. https://doi.org/10.1016/j.epsl.2018.05.038.

Muratli, J.M., Polyak, L., Haley, B.A., Kuznetsov, A., 2022. North American glaciations and Pacific inputs in the Nd and Sr isotope Pleistocene record from the western Arctic Ocean. Paleoceanogr. Paleoclimatol. https://doi.org/10.1029/2022PA004479.

Naafs, B.D.A., Hefter, J., Grützner, J., Stein, R., 2013. Warming of surface waters in the mid-latitude North Atlantic during Heinrich events. Paleoceanography 28, 153–163. https://doi.org/10.1029/2012PA002354.

Pasquier, B., Hines, S.K.V., Liang, H., Wu, Y., Goldstein, S.L., John, S.G., 2022. GNOM v1.0: an optimized steady-state model of the modern marine neodymium cycle. Geosci. Model Dev. (GMD) 15, 4625–4656. https://doi.org/10.5194/gmd-15-4625-2022.

Pena, L.D., Goldstein, S.L., 2014. Thermohaline circulation crisis and impacts during the mid-Pleistocene transition. Science (345), 318–322. https://doi.org/10.1126/science.1249770, 1979.

Peterson, C.D., Lisiecki, L.E., Stern, J.V., 2014. Deglacial whole-ocean $\delta^{13}C$ change estimated from 480 benthic foraminiferal records. Paleoceanogr. Paleoclimatol. 29, 549–563. https://doi.org/10.1002/2013PA002552.

Piotrowski, A.M., Banakar, V.K., Scrivner, A.E., Elderfield, H., Galy, A., Dennis, A., 2009. Indian Ocean circulation and productivity during the last glacial cycle. Earth Planet Sci. Lett. 285, 179–189. https://doi.org/10.1016/j.epsl.2009.06.007.

Pöppelmeier, F., Gutjahr, M., Blaser, P., Keigwin, L.D., Lippold, J., 2018. Origin of abyssal NW atlantic water masses since the last glacial maximum. Paleoceanogr. Paleoclimatol. 17, 530–543. https://doi.org/10.1029/2017PA003290.

Pöppelmeier, Frerk, Scheen, J., Blaser, P., Lippold, J., Gutjahr, M., Stocker, T.F., 2020a. Influence of elevated Nd fluxes on the northern Nd isotope end member of the atlantic during the early Holocene. Paleoceanogr. Paleoclimatol. 35. https://doi.org/10.1029/2020PA003973.

Pöppelmeier, F., Blaser, P., Gutjahr, M., Jaccard, S.L., Frank, M., Max, L., Lippold, J., 2020b. Northern-sourced water dominated the Atlantic Ocean during the last glacial maximum. Geology 48, 826–829. https://doi.org/10.1130/G47628.1.

Pöppelmeier, F., Gutjahr, M., Blaser, P., Schulz, H., Süfke, F., Lippold, J., 2021. Stable Atlantic Deep Water Mass Sourcing on Glacial-Interglacial Timescales. Geophys Res Lett 48, pp. 1–10. https://doi.org/10.1029/2021GL092722.

Pöppelmeier, F., Lippold, J., Blaser, P., Gutjahr, M., Frank, M., Stocker, T.F., 2022. Neodymium isotopes as a paleo-water mass tracer: a model-data reassessment. Quat. Sci. Rev. 279, 107404. https://doi.org/10.1016/j.quascirev.2022.107404.

Pöppelmeier, F., Jeltsch-Thömmes, A., Lippold, J., Joos, F., Stocker, T.F., 2023. Multi-proxy constraints on Atlantic circulation dynamics since the last ice age. Nat. Geosci. 16, 349–356. https://doi.org/10.1038/s41561-023-01140-3.

Rahlf, P., Hathorne, E., Laukert, G., Gutjahr, M., Weldeab, S., Frank, M., 2020. Tracing water mass mixing and continental inputs in the southeastern Atlantic Ocean with dissolved neodymium isotopes. Earth Planet Sci. Lett. 530, 115944. https://doi.org/10.1016/j.epsl.2019.115944.

Raymo, M.E., Oppo, D.W., Flower, B.P., Hodell, D.A., McManus, J.F., Venz, K.A., Kleiven, K.F., McIntyre, K., 2004. Stability of North Atlantic water masses in face of pronounced climate variability during the Pleistocene. Paleoceanography 19, PA2008. https://doi.org/10.1029/2003PA000921.

Raymo, M.E., Ruddiman, W.F., Shackleton, N.J., Oppo, D.W., 1990. Evolution of Atlantic-Pacific $\delta^{13}C$ gradients over the last 2.5 m.y. Earth Planet Sci. Lett. 97, 353–368. https://doi.org/10.1016/0012-821X(90)90051-X.

Raymo, M.E., Oppo, D.W., Curry, W., 1997. The mid-Pleistocene climate transition: a deep sea carbon isotope perspective. Paleoceanogr. Paleoclimatol. 12, 546–559. https://doi.org/10.1029/97PA01019.

Raymo, M.E., Lisiecki, L.E., Nisancioglu, K.H., 2006. Plio-pleistocene ice volume, antarctic climate, and the global $\delta^{18}O$ record. Science 313, 492–495. https://doi.org/10.1126/science.1123296.

Roberts, N.L., Piotrowski, A.M., McManus, J.F., Keigwin, L.D., 2010. Synchronous deglacial overturning and water mass source changes. Science 327, 75–78. https://doi.org/10.1126/science.1178068, 1979.

Robinson, S., Ivanovic, R., van de Flierdt, T., Blanchet, C.L., Tachikawa, K., Martin, E.E., Cook, C.P., Williams, T., Gregoire, L., Plancherel, Y., Jeandel, C., Arsouze, T., 2021. Global Continental and Marine Detrital εNd: an Updated Compilation for Use in Understanding Marine Nd Cycling. Chem Geol 567, 120119. https://doi.org/10.1016/j.chemgeo.2021.120119.

Robinson, S., Ivanovic, R.F., Gregoire, L.J., Tindall, J., van de Flierdt, T., Plancherel, Y., Pöppelmeier, F., Tachikawa, K., Valdes, P.J., 2023. Simulating marine neodymium isotope distributions using Nd v1.0 coupled to the ocean component of the FAMOUS–MOSES1climate model: sensitivities to reversible scavenging efficiency and benthic source distributions. Geosci. Model Dev. (GMD) 16, 1231–1264. https://doi.org/10.5194/gmd-16-1231-2023.

Rodriguez-Sanz, L., Mortyn, P.G., Martinez-Garcia, A., Rosell-Mele, A., Hall, I.R., 2012. Glacial Southern Ocean Freshening at the Onset of the Middle Pleistocene Climate Transition. Earth Planet Sci Lett 345-348, pp. 194–202. https://doi.org/10.1016/j.epsl.2012.06.016.

Rohling, E.J., Foster, G.L., Grant, K.M., Marino, G., Roberts, A.P., Tamisiea, M.E., Williams, F., 2014. Sea-level and deep-sea-temperature variability over the past 5.3 million years. Nature 508, 4477–4482. https://doi.org/10.1038/nature13230.

Roy, M., Clark, P.U., Raisbeck, G.M., Yiou, F., 2004. Geochemical constraints on the regolith hypothesis for the middle Pleistocene transition. Earth Planet Sci. Lett. 227, 281–296. https://doi.org/10.1016/j.epsl.2004.09.001.

Smith, M.E., Glick, E.V., Lodestro, S., Rashid, H., 2013. Data report: oxygen isotopes and foraminifer abundance record for the last glacial-interglacial cycle and marine isotope Stage 6 at IODP Site U1313. In: https://doi.org/10.2204/iodp.proc.303306.216.2013.

Starr, A., Hall, I.R., Barker, S., Rackow, T., Zhang, X., Hemming, S.R., van der Lubbe, H.J.L., Knorr, G., Berke, M.A., Bigg, G.R., Cartagena-Sierra, A., Jiménez-Espejo, F.J., Gong, X., Gruetzner, J., Lathika, N., LeVay, L.J., Robinson, R.S., Ziegler, M., Brentegani, L., Caley, T., Charles, C.D., Coenen, J.J., Crespin, J.G., Franzese, A.M., Han, X., Hines, S.K.V., Jimenez Espejo, F.J., Just, J., Koutsodendris, A., Kubota, K., Norris, R.D., dos Santos, T.P., Rolison, J.M., Simon, M.H., Tangunan, D., van der Lubbe, H.J.L., Yamane, M., Zhang, H., 2021. Antarctic icebergs reorganize ocean circulation during Pleistocene glacials. Nature 589, 236–241. https://doi.org/10.1038/s41586-020-03094-7.

Struve, T., Roberts, N.L., Frank, M., Piotrowski, A.M., Spielhagen, R.F., Gutjahr, M., Teschner, C., Bauch, H.A., 2019. Ice-sheet driven weathering input and water mass mixing in the Nordic Seas during the last 25,000 years. Earth Planet. Sci. Lett. 514, 108–118. https://doi.org/10.1016/j.epsl.2019.02.030.

Tachikawa, K., Arsouze, T., Bayon, G., Bory, A., Colin, C., Dutay, J.C., Frank, N., Giraud, X., Gourlan, A.T., Jeandel, C., Lacan, F., Meynadier, L., Montagna, P., Piotrowski, A.M., Plancherel, Y., Pucéat, E., Roy-Barman, M., Waelbroeck, C., 2017. The large-scale evolution of neodymium isotopic composition in the global modern and Holocene ocean revealed from seawater and archive data. Chem. Geol. 457, 131–148. https://doi.org/10.1016/j.chemgeo.2017.03.018.

Tachikawa, K., Rapuc, W., Vidal, L., Dubois-dauphin, Q., P, N., Deschamps, P., Skonieczny, C., 2021. Eastern Atlantic deep-water circulation and carbon storage inferred from neodymium and carbon isotopic compositions over the past 1.1 million years. Quat. Sci. Rev. 252, 106752. https://doi.org/10.1016/j.quascirev.2020.106752.

Tanaka, T., Togashi, S., Kamioka, H., Amakawa, H., Kagami, H., Hamamoto, T., Yuhara, M., Orihashi, Y., Yoneda, S., Shimizu, H., Kunimaru, T., Takahashi, K., Yanagi, T., Nakano, T., Fujimaki, H., Shinjo, R., Asahara, Y., Tanimizu, M., Dragusanu, C., 2000. JNdi-1: a neodymium isotopic reference in consistency with LaJolla neodymium. Chem. Geol. 168, 279–281. https://doi.org/10.1016/S0009-2541(00)00198-4.

van de Flierdt, T. Van De, Griffiths, A.M., Lambelet, M., Little, S.H., Stichel, T., Wilson, D. J., 2016. Subject Areas : neodymium in the oceans : a global database , a regional comparison and implications for palaeoceanographic research. Philosophical Transactions of the Royal Society A 374. https://doi.org/10.1098/rsta.2015.0293.

von Blanckenburg, F., Bouchez, J., Ibarra, D.E., Maher, K., 2015. Stable runoff and weathering fluxes into the oceans over Quaternary climate cycles. Nat. Geosci. 8, 538–542. https://doi.org/10.1038/ngeo2452.

Wang, R., Clegg, J.A., Scott, P.M., Larkin, C.S., Feng, F., Thomas, A.L., Zheng, X.-Y., Piotrowski, A.M., 2021. Geochim Cosmochim Acta 314, 121–139. https://doi.org/10.1016/j.gca.2021.09.015.

Willeit, M., Ganopolski, A., Calov, R., Brovkin, V., 2019. Mid-Pleistocene transition in glacial cycles explained by declining CO2 and regolith removal. Sci. Adv. 5, 1–9. https://doi.org/10.1126/sciadv.aav7337.

Williams, T.J., Martin, E.E., Sikes, E., Starr, A., Umling, N.E., Glaubke, R., 2021. Neodymium isotope evidence for coupled Southern Ocean circulation and Antarctic climate throughout the last 118,000 years. Quat. Sci. Rev. 260, 106915. https://doi.org/10.1016/j.quascirev.2021.106915.

Wilson, D.J., Piotrowski, A.M., Galy, A., Banakar, V.K., 2015. Interhemispheric controls on deep ocean circulation and carbon chemistry during the last two glacial cycles. Paleoceanography 30 (6), 621–641. https://doi.org/10.1002/2014PA002707.

Wu, Y., Pena, L.D., Anderson, R.F., Hartman, A.E., Bolge, L.L., Basak, C., Kim, J., Rijkenberg, M.J.A., de Baar, H.J.W., Goldstein, S.L., 2022. Assessing neodymium isotopes as an ocean circulation tracer in the Southwest Atlantic. Earth Planet Sci. Lett. 599. https://doi.org/10.1016/j.epsl.2022.117846.

Yehudai, M., Kim, J., Pena, L.D., Jaume-Seguí, M., Knudson, K.P., Bolge, L., Malinverno, A., Bickert, T., Goldstein, S.L., 2021. Evidence for a Northern Hemispheric trigger of the 100,000-y glacial cyclicity. Proc. Natl. Acad. Sci. USA 118, e2020260118. https://doi.org/10.1073/pnas.2020260118.

Yehudai, M., Tweed, L.E., Ridge, S., Wu, Y., Goldstein, S.L., 2023. Effects of past Nd seawater concentrations on Nd-isotope paleocirculation reconstructions: a bayesian approach. Geophys. Res. Lett. 50, e2023GL104489. https://doi.org/10.1029/2023GL104489.

Zhao, N., Oppo, D.W., Huang, K.F., Howe, J.N.W., Blusztajn, J., Keigwin, L.D., 2019. Glacial–interglacial Nd isotope variability of North Atlantic Deep Water modulated by North American ice sheet. Nat. Commun. 10, 1–10. https://doi.org/10.1038/s41467-019-13707-z.